In vivo bone strain and finite element modeling of the mandible of *Alligator mississippiensis*

Laura B. Porro,[1,2] Keith A. Metzger,[3] Jose Iriarte-Diaz[1] and Callum F. Ross[1]

[1]Department of Organismal Biology and Anatomy, University of Chicago, Chicago, IL, USA
[2]School of Earth Sciences, University of Bristol, Bristol, UK
[3]Department of Science Education, Hofstra North Shore – LIJ School of Medicine, Hempstead, NY, USA

Abstract

Forces experienced during feeding are thought to strongly influence the morphology of the vertebrate mandible; *in vivo* strain data are the most direct evidence for deformation of the mandible induced by these loading regimes. Although many studies have documented bone strains in the mammalian mandible, no information is available on strain magnitudes, orientations or patterns in the sauropsid lower jaw during feeding. Furthermore, strain gage experiments record the mechanical response of bone at a few locations, not across the entire mandible. In this paper, we present bone strain data recorded at various sites on the lower jaw of *Alligator mississippiensis* during *in vivo* feeding experiments. These data are used to understand how changes in loading regime associated with changes in bite location are related to changes in strain regime on the working and balancing sides of the mandible. Our results suggest that the working side mandible is bent dorsoventrally and twisted about its long-axis during biting, and the balancing side experiences primarily dorsoventral bending. Strain orientations are more variable on the working side than on the balancing side with changes in bite point and between experiments; the balancing side exhibits higher strain magnitudes. In the second part of this paper, we use principal strain orientations and magnitudes recorded *in vivo* to evaluate a finite element model of the alligator mandible. Our comparison demonstrates that strain orientations and mandibular deformation predicted by the model closely match *in vivo* results; however, absolute strain magnitudes are lower in the finite element model.

Key words: biomechanics; crocodilians; feeding; validation.

Introduction

Understanding the extent to which combinations of external forces (*loading regimes*) acting on the skeleton are associated with internal *stress, strain* and *deformation regimes* is fundamental in evaluating hypotheses regarding form–function relationships and is an important objective of biomechanics, functional morphology and vertebrate paleontology (Bock & Von Wahlert, 1965; Plotnick & Baumiller, 2000; Schwenk, 2000). Moreover, obtaining such data from several taxa can be used to relate interspecific differences in skeletal morphology to differences in behavior, habitat or diet.

The vertebrate mandible is an important structure in which to investigate the association between loading regime and stress and strain regimes because of its role in

feeding, during which it transmits forces to and from the organism and environment. Relationships between *in vivo* loading regimes, strain regimes and mandibular morphology have been examined in numerous mammalian taxa, including rabbits (Weijs & De Jongh, 1977), pigs (Liu & Herring, 2000; Herring et al. 2001), hyraxes (Lieberman et al. 2004), selenodont artiodactyls (Williams et al. 2008, 2009) and primates (Hylander, 1979b, 1981, 1984; Hylander et al. 1987, 1998), but we know of no published *in vivo* bone strain studies examining the sauropsid (Testudines + Squamates + Archosaurs) lower jaw. As a result, comparative hypotheses regarding the functional significance of variation in mandibular morphology across vertebrates are currently limited (but see Hylander & Crompton, 1986). Additionally, numerous morphological features characteristic of sauropsids, including the presence of mandibular sutures, a mandibular fenestra, and lack of adductor musculature lateral to the mandibular ramus, are absent in mammals, making extrapolation of sauropsid mandibular function from mammalian studies tenuous (Weishampel, 1995). Documenting *in vivo* mechanical behavior of the *Alligator* mandible is a first step towards understanding

sauropsid jaw biomechanics, and takes the study of feeding function in reptiles beyond the realm of theoretical analyses. Furthermore, the extreme bite forces reported in crocodilians (Erickson et al. 2003, 2012) and high strain magnitudes recorded from the *Alligator* cranium (Ross & Metzger, 2004) suggest that feeding may exert particularly strong selective pressure on mandibular morphology in crocodilians.

Cranial mechanical behavior in various extant and extinct sauropsids has been modeled using different techniques (Busbey, 1995; Daniel & McHenry, 2001; Metzger et al. 2005; McHenry et al. 2006; Rayfield et al. 2007; Pierce et al. 2008; Rayfield & Milner, 2008; Moazen et al. 2009; Soons et al. 2010); in contrast, the sauropsid mandible has received little attention. Studies of sauropsid mandibular function include: free-body analyses of crocodilian, dinosaur and bird mandibles (Bock, 1966; Van Drongelen & Dullemeijer, 1982; Molnar, 1998); beam modeling of plesiosaur, crocodilian and theropod dinosaur mandibles (Taylor, 1992; Therrien et al. 2005; Porro et al. 2011); photoelastic studies of bird mandibles (Bock & Kummer, 1968) and finite element analysis (FEA) of the mandibles of *Varanus*, *Alligator*, several dinosaur taxa, and ostrich (Mazzetta et al. 2004; Moreno et al. 2008; Bell et al. 2009; Porro et al. 2011; Rayfield, 2011; Reed et al. 2011). FEA is a useful tool for understanding the mechanical behavior of geometrically and materially complex structures that cannot be adequately modeled using simpler methods. FEA also has advantages over strain gage experiments: strain can be calculated in places inaccessible to gages; strain can be observed throughout the entire structure rather than at a limited number of sites; and three-dimensional internal strains are recorded in addition to surface strains. Furthermore, FEA can be used to test the mechanical significance of anatomical features by generating hypothetical structures (Strait et al. 2007; Rayfield & Milner, 2008) and revealing the mechanical behavior of extinct sauropsid skulls (Rayfield et al. 2001, 2007; Bell et al. 2009; Mazzetta et al. 2009).

Results generated by FEA should be evaluated against *in vivo/in vitro* strain data both to appraise the accuracy of model predictions (*validation*) and to determine how variability in input parameters impacts model results (*sensitivity analyses*). Validation studies comparing the behavior of finite element model (FEM) skulls with *in vivo/in vitro* results have been largely confined to mammals (Verrue et al. 2001; Ross et al. 2005, 2011; Strait et al. 2005; Kupczik et al. 2007; Bright & Rayfield, 2011; Panagiotopoulou et al. 2011). An FEM of the *Alligator* cranium is the only non-mammalian skull for which a validation study has been carried out (Metzger et al. 2005) and no model of a sauropsid mandible has yet been validated against *in vivo* strain data (see (Rayfield, 2011) comparing *in vitro* bone strains and FEA in the ostrich). Although previous studies have used FEA to predict overall mandibular deformation in the *Alligator* mandible (Porro et al. 2011) and quantify model sensitivity to input parameters (Reed et al. 2011), it is unclear how well model predictions reflect reality without validation.

The goals of this study are: (i) to document patterns of *in vivo* bone strain in the *Alligator* mandible during biting, including variance in strain patterns at multiple gage sites during biting at different points along the tooth row on the working (biting) and balancing (non-biting) sides and calculation of the neutral axis of bending in a transverse section of the mandible; (ii) to use *in vivo* bone strain data to validate a high resolution FEM of the *Alligator* mandible; (iii) to use the FEM to predict overall patterns of deformation and strain in the *Alligator* mandible during biting at different points along the toothrow; and (iv) to compare *Alligator* mandibular strain regimes with those collected from mammals.

Material and methods

In vivo bone strain recording and analysis

Subjects

Three sub-adult American alligators (*Alligator mississippiensis*; head length 12.3, 20.5, and 17.5 cm) were used in five separate experiments. Animals were individually housed in large enclosures with wet and dry areas on a 12-h light/dark cycle and fed mice, chicken and fish three times per week. Environmental temperature ranged from 28 °C during the day to 20 °C at night and water was kept at a constant temperature of 27 °C using a submersible heater. Animals were housed in the Stony Brook University Division of Laboratory Animal Resources in accordance with the National Institutes of Health Guidelines for the Care and Use of Laboratory Animals. All experimental procedures were approved by the Stony Brook University Institutional Animal Care and Use Committee.

Bone strain data collection

During experiments, stacked delta rosette strain gages (SA-06-030WY-120; Micromeasurements, Raleigh, NC) or rectangular rosette strain gages (FRA 1-11-1L; Texas Measurements, Inc., College Station, TX) were wired, insulated, and gas-sterilized using previously described procedures (Ross, 2001). Following anesthesia with 2% isofluorane administered in oxygen through an intubation tube, 1 cm² of skin overlying the gage sites was removed, the periosteum elevated, the bone degreased with chloroform, and the gage bonded to the surface of the bone using cyanoacrylate adhesive. Gages were placed in multiple locations during five separate experiments, including the dorsolateral, lateral and ventral surfaces of the dentary, ventral and medial surfaces of the splenial, and the angular (Table 1, Fig. 1). Gage lead wires were epoxied and sutured to the skin overlying the mandible to provide strain relief and secured to the back of the animal with veterinary tape. Following surgery, all animals were radiographed to obtain a permanent record of strain gage locations.

Animals recovered from surgery for at least 2 h before strains were recorded while the animal bit unilaterally on steel bite plates covered with several layers of surgical tape. The upper layer was replaced after each bite so that bite position was accurately

Table 1 Experimental summary including strain gage locations by experiment. For gages with nearly identical placement in different experiments, only one site was analyzed in the FEM.

Experiment ID number	Animal ID	Mandible side	Gage location	FEM gage ID number
56	1	Right	Anterior ventral dentary	1
			Posterior ventral dentary	2
			Ventral angular	3
75	1	Left	Lateral dentary	4
			Ventral dentary	5
			Medial splenial	6
99	2	Right	Dorsolateral dentary	7
			Lateral dentary	4
			Ventral dentary	5
			Medial splenial	6
102	3	Left	Dorsolateral dentary	8
			Lateral dentary	9
			Ventral dentary	10
			Ventral splenial	11
			Medial splenial	12
103	3	Right	Dorsolateral dentary	7
			Lateral dentary	13
			Ventral dentary	1
			Medial splenial	14

recorded using tooth impressions. To investigate variance in strain patterns with changes in bite point, the location of each recorded bite was assigned to one of 10 equal-sized regions of the mandible: left or right anterior, anterior/middle, middle, middle/posterior, and posterior regions (Fig. 1) (additionally, strains were recorded during biting at the midline anterior end of the jaws; results for these bites are presented in Tables 2–6 but not discussed). Biting side and location as well as the presence of any unusual activity (shake, attempted twisting) were recorded on a data sheet; data from these activities were excluded from the present study.

Voltage changes in the gages were conditioned and amplified on Vishay 2100 bridge-amplifiers. Data were acquired at 1 kHz through a National Instruments DAQ board run by MIDAS data acquisition software package (Xcitex, Cambridge, MA) and saved to a PC.

In vivo bone strain data analysis

In vivo strain data were filtered and processed in IGOR PRO 4.0 (Wave-Metrics, Inc., Lake Oswego, OR) using custom-written software. The strain data (strain is a dimensionless unit, ε, that represents change in length over original length or $\Delta L/L$) were converted to micro-strain ($\mu\varepsilon$, which are equal to 1×10^{-6} inches per inch or mm per mm) using calibration files produced during the recording sessions. The magnitude of maximum (ε_1) and minimum (ε_2) principal strains were calculated (Hibbeler, 2000) (Tables 2–6). Maximum principal strain (ε_1) is usually the largest tensile strain value, and the minimum principal strain is usually the largest compressive strain value (ε_2). The ratios of maximum to minimum principal strains ($|\varepsilon_1/\varepsilon_2|$) were calculated (Tables 2–6) as was shear strain (γ), which is equal

to $|\varepsilon_1 - \varepsilon_2|$. The orientations of the maximum principal strains (ε_1) were also calculated (Tables 2–6). For consistency, ε_1 orientations for *in vivo* experiments and the FEM (as presented in tables and vector plots, as well as those used in statistical analyses) are calculated for a right mandible. The orientation of ε_1 in lateral, medial and ventral views were calculated relative to a reference axis aligned between the most anterior point of the external mandibular fenestra to the posterior base of the sixth dentary tooth; the reference plane was defined by this axis and another line parallel to either the ventral (for medial and lateral views) or medial (for ventral view) border of the mandible (Fig. 1). Converting strain orientations to this common reference axis enables comparisons between different experiments and between *in vivo* and FEM data. By convention, positive values are those rotated counterclockwise from the reference axis (vectors rotated clockwise from the axis are negative) when viewed from the right (for medial and lateral views) or from below (for ventral view). Custom software in IGOR PRO 4.0 was used to convert strain orientations and magnitudes to vectors within polar coordinates. Vector plots (Figs 2 and 3), in which the relative magnitudes and orientations of ε_1 for all gage sites during all recorded bites are displayed, were created using ADOBE ILLUSTRATOR CS 5.1 (Adobe System Incorporated, San Jose, CA).

Data from experiments in which three gages were placed around the circumference of the lower jaw allow normal strain distribution to be reconstructed at the section of the gages. From this distribution, maximum and minimum normal strains for the cross-section can be calculated (Rybicki et al. 1977; Demes et al. 2001; Demes, 2007). This gives an indication of the maximum tensile and compressive strains experienced in the section and allows the orientation of the neutral axis within the cross-section to be determined. The orientation of the neutral axis was calculated using data from four experiments (75, 99, 102 and 103) in which there were three or more gages placed around the circumference of the mandible in a coronal plane. To calculate the orientation of the neutral axis of bending, normal strains (strains normal to the plane of the cross-section) were calculated from peak principal strains recorded during each bite. Orientation of the neutral axis is reliant upon both normal strains and bone cross-sectional geometry (Rybicki et al. 1977; Carter et al. 1981; Demes, 2007). The orientation of the neutral axis was determined using the formula:

$$\tan = \alpha = (I_{\max}/I_{\min})/\tan \theta \qquad (1)$$

where α = angle of the neutral axis with maximum principal axis, θ = angle of external bending direction with maximum principal axis, and $I_{\max, \min}$ = maximum and minimum principal moments of cross-section (Hibbeler, 2000). Cross-sectional geometry of the mandible was determined from postmortem CT scans of the specimens. Normal strains were calculated assuming that material properties are homogeneous through the cross-section and that sutures do not dissipate or reorient strains. Calculations of normal strains and neutral axis were conducted using a custom macro for IGOR PRO provided by B. Demes, Stony Brook University.

Finite element analysis

Model construction

Strain data collected *in vivo* were compared with predictions from a high-resolution FEM of the *Alligator* mandible; additionally, the FEM was used to relate the *in vivo* strain data to global strain patterns and deformation throughout the *Alligator* mandible. The FEM described here has been used previously to understand the
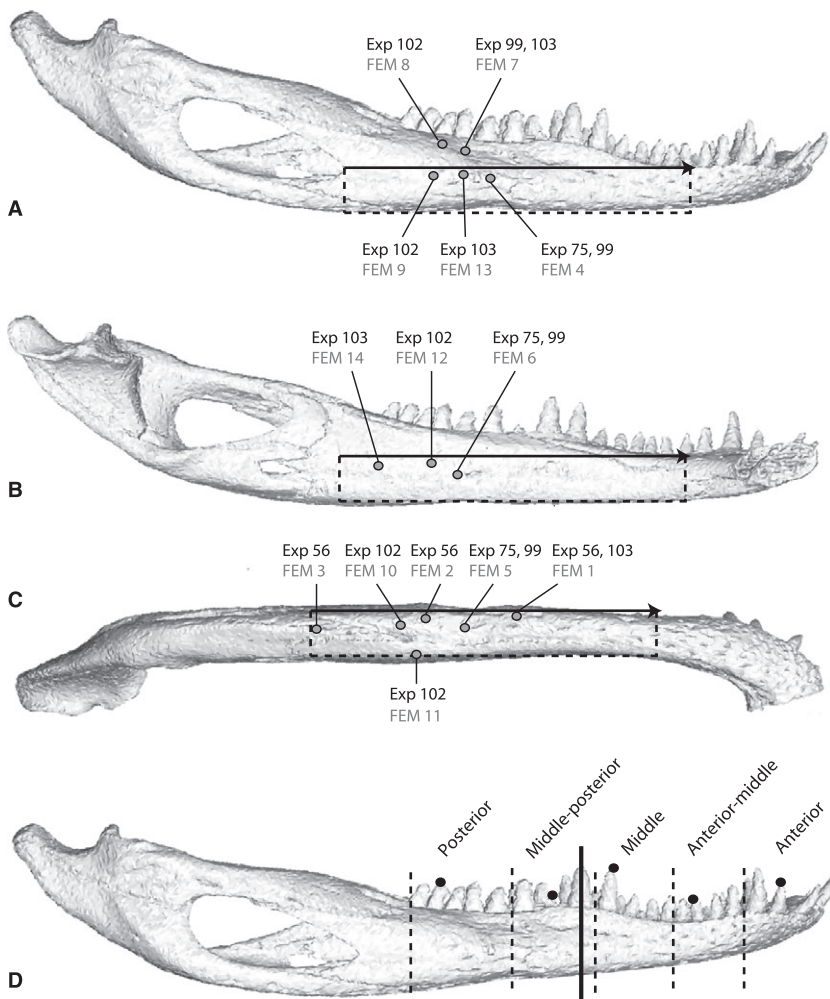
Fig. 1 Gage locations, reference axes and bite points. The mandible of the *Alligator* in lateral (A), medial (B) and ventral (C) views illustrating the locations of experimental strain gages (black text) and equivalent areas in the FEM (finite element model) (gray text). The reference axis used to standardize strain orientations across all experiments and the FEM is shown in all three views as a black arrow from the anterior point of the external mandibular fenestra to the posterior base of the 6th dentary tooth; strains rotated counterclockwise from this axis are positive, those rotated clockwise are negative. Dotted lines in A, B and C indicate the reference planes. Bite locations during *in vivo* experiments (dotted lines) and constraints in the FEM (black dots) are shown in (D). The solid black line in (D) indicates the section used to determine axis of bending in the FEM.

impact of material properties on mandible deformation (Reed et al. 2011) and has been compared with results from simpler beam modeling and free-body analyses (Porro et al. 2011).

The preserved head (mandibular length of 189 mm) of one of the individuals used in our experiments was CT scanned at Stony Brook University Medical Center using a GE LightSpeed 16 CT scanner at 100 kV per 70 mA to produce 645 coronal slices with a slice thickness of 0.31 mm and a resolution of 0.25 mm per pixel. Scans were segmented in AMIRA 5.2.2 (Visage Imaging GmbH, Berlin, Germany) to generate a 3D surface model in which individual mandibular bones, sutures, periodontal ligament, and teeth were treated as separate parts; the cranium, including all bones and teeth, was segmented as a single part. The surface model was meshed with linear tetrahedra in the finite element software package STRAND7 2.4.1 (Strand7 Pty Ltd, Sydney, Australia) and the jaws of the model set at a gape angle of 30°.

The attachment sites of 16 jaw elevator muscles (the superficial, medial and deep portions of the external adductor; superficial and deep pseudotemporalis; posterior adductor; and dorsal and ventral portions of the pterygoideus on both sides of the head), and depressor mandibulae, were mapped onto the skull using information from dissections and the literature (Holliday & Witmer, 2007). The reduced physiological cross-sectional area (PCSA), accounting for muscle mass, pinnation, and fiber and sarcomere lengths, was determined for each muscle (Porro et al. 2011); reduced PCSA was multiplied by 300 kN m^{-2} to yield the maximum contractile force generated by each muscle (Sinclair & Alexander, 1987). Muscle forces were loaded onto the FEM using the VISUAL BASIC script BONELOAD (Grosse et al. 2007) which accounts for tensile, tangential and normal traction loads due to muscles wrapping around bone surfaces. The model was constrained at three nodes aligned mediolaterally across the joint surfaces of the quadrates (cranium) and articulars (mandible), preventing rigid body motion and generating joint reaction forces. Additionally, the tip of a single right dentary tooth (and its closest opposing premaxillary or maxillary tooth) was fixed to generate bite force. Five loading conditions were analyzed: anterior (3rd tooth), anterior-middle (7th tooth), middle (12th tooth), middle-posterior (14th tooth), and posterior (19th tooth) bite points, corresponding to similar areas in *in vivo* experiments. In all cases, the right side of the FEM was the working side and the left side was the balancing side. A single node was constrained on the medial surface of each mandible (opposite its contact with the pterygoid flange) to restrict medial bending and torsion of the mandibular ramus (the importance of this constraint is described in Porro et al. 2011).

Alligator mandibular bone properties applied to the FEM were obtained from an individual similar in size to the animals used in our experiment (Zapata et al. 2010; Porro et al. 2011). Mandibular sutures and periodontal ligament were assigned a density and Poisson's ratio reflecting the average reported in the literature (Currey,

Table 2 Descriptive statistics for principal (ε_1 and ε_2) and $|(\varepsilon_1/\varepsilon_2)|$ strain magnitude and ε_1 orientation for Experiment 56.

Gauge location	Bite side	Bite position	n	ε_1 Mean	SD	Max.	ε_2 Mean	SD	Max.	$\varepsilon_1/\varepsilon_2$ ratio Mean	SD	ε_1 orientation Mean	SD
Right ventral angular	Left (BS)	a	4	71	45	122	−120	49	−148	0.61	0.27	113	33
		p	5	56	21	88	−129	41	−183	0.48	0.25	101	28
	All left		9	63	34	122	−125	42	−183	0.54	0.25	107	28
	Right (WS)	a/m	2	35	31	57	−205	158	−317	0.16	0.03	66	3
		m	4	15	10	26	−178	27	−202	0.08	0.06	73	13
		m/p	1	3		3	−273			0.01		72	
		p	6	14	4	20	−206	61	−314	0.07	0.03	66	6
	All right		13	17	14	57	−202	67	−314	0.09	0.05	69	9
	All bites		22	34	31	122	−163	70	−317	0.27	0.27	85	27
Right anterior dentary	Midline		2	426	193	563	−648	354	−899	0.68	0.07	110	7
	Left (BS)	a	4	779	291	1003	−1076	476	−1487	0.75	0.09	−1	1
		p	6	457	149	703	−568	230	−962	0.82	0.05	6	4
	All left		10	600	257	1003	−794	403	−1487	0.79	0.07	3	4
	Right (WS)	a/m	2	782	117	865	−570	53	−608	1.37	0.08	−25	2
		m	4	816	319	1244	−908	426	−1427	0.94	0.13	−40	11
		m/p	1	952		952	−819		−819	1.16		−29	
		p	6	543	165	830	−443	156	−744	1.24	0.17	−21	3
	All right		13	695	247	1244	−634	320	−1427	1.16	0.21	−28	10
	All bites		22	637	254	1244	−695	359	−1487	0.98	0.26	0	53
Right posterior dentary	Midline		2	37	28	56	−81	12	−89	0.43	0.28	−33	8
	Left (BS)	a	4	125	45	182	−77	29	−105	1.65	0.16	12	6
		p	6	118	30	142	−95	29	−140	1.36	0.51	20	24
	All left		10	121	47	182	−87	26	−140	1.49	0.4	17	19
	Right (WS)	a/m	2	54	16	65	−47	30	−68	1.57	1.33	−12	14
		m	4	176	61	218	−209	73	−281	0.84	0.09	−27	2
		m/p	1	139			−226		−226	0.62		−25	
		p	6	159	62	238	−229	118	−318	0.76	0.15	−29	1
	All right		13	147	66	238	−195	107	−318	0.9	0.5	−26	8
	All bites		22	128	61	238	−145	97	−318	1.08	0.56	−13	54

a, anterior; a/m, anterior/middle; m, middle; m/p, middle/posterior; p, posterior.

2002; Kupczik et al. 2007). Material properties for bone were anisotropic: X refers to the mediolateral axis, Y to the dorsoventral axis, and Z to the anteroposterior axis of the mandible. The following properties were applied to the model: bone [density of 1662.8 kg m^{-3}; elastic moduli of 8.1 GPA (X), 9.26 GPA (Y) and 19.71 GPA (Z); shear moduli of 3.17 GPA (XY), 4.45 GPA (XZ), and 5.51 GPA (YZ); Poisson's ratios of 0.38 (XY), 0.08 (XZ), and 0.15 (YZ)]; teeth (density of 2076 kg m^{-3}; elastic modulus of 21 GPA; Poisson's ratio of 0.31); sutures and periodontal ligament (density of 1200 kg m^{-3}; elastic modulus of 0.09 GPA; Poisson's ratio of 0.3). The FEM was solved using the linear static solver in STRAND7.

In silico strain data extraction

Prior to analysis, bricks on the surface of the FEM most closely corresponding to gage sites in the experiments were identified on both the working (right) and balancing (left) sides. The three-dimensional 2nd-order strain tensor of each brick within these sites were exported from STRAND7 to MATLAB (MathWorks, Nantick, MA) where custom-written code (Ross et al. 2011) was used to calculate the magnitude and orientation of the maximum and minimum principal surface strains in the FEM (Table 7). The orientations of the ε_1 surface strains were transformed relative to the reference axis

described above using MATLAB, and strain orientations and magnitudes converted to vectors within polar coordinates in IGOR PRO 4.0, making ε_1 orientations from the FEM and *in vivo* experiments directly comparable (Table 7). Vectors representing the mean ε_1 orientation of all bricks within a gage site during anterior and posterior biting are superimposed over *in vivo* data in vector plots (Figs 2 and 3). Additionally, the ratio of maximum to minimum principal strains ($|\varepsilon_1/\varepsilon_2|$) and maximum shear strain (γ-max) were calculated for FEM gage sites.

To determine the neutral axis of bending in the FEM, cross-sections of the working and balancing sides at the level of the 13th dentary tooth were analyzed for strain perpendicular to the section. For each bite point, contour plots were used to determine the orientation of the neutral axis and the maximum and minimum principal strains within the section.

In vivo and FEM bone strain data statistical analyses

To quantify the effect of bite point on strain in the mandible, data were split into the 10 toothrow regions described above. On all data tables for *in vivo* experiments (Tables 2–6), missing data indicate that no strains were recorded for a particular bite position.

Table 3 Descriptive statistics for principal (ε_1 and ε_2) and $|(\varepsilon_1/\varepsilon_2)|$ strain magnitude and ε_1 orientation for experiment 75.

Gauge location	Bite side	Bite position	n	ε_1 Mean	SD	Max	ε_2 Mean	SD	Max	$\varepsilon_1/\varepsilon_2$ Ratio Mean	SD	ε_1 Orientation Mean	SD
Left lateral dentary	Left (WS)	a/m	4	1098	420	1434	−1131	449	−1389	0.98	0.08	−37	6
		m	6	530	271	848	−387	321	−961	1.66	0.44	−29	12
		m/p	12	1379	976	2846	−976	786	−2006	1.88	0.85	−35	9
		p	8	1006	382	1386	−615	283	−1003	1.79	0.45	−41	8
	All left		30	1073	727	2846	−783	604	−2006	1.69	0.67	−36	9
	Right (BS)	a	4	648	90	731	−453	58	−492	1.43	0.04	31	2
		a/m	3	1328	203	1543	−983	179	−1172	1.36	0.04	33	1
		m	19	1492	290	1868	−1157	248	−1481	1.3	0.04	34	1
		m/p	7	946	508	1728	−714	427	−1388	1.37	0.12	33	3
		p	15	1191	446	1714	−893	352	−1325	1.35	0.07	32	2
	All right		48	1238	443	1868	−941	365	−1481	1.34	0.07	33	2
	All bites		78	1174	571	2846	−880	474	−2006	1.48	0.45	2	34
Left ventral dentary	Left (WS)	a/m	4	924	488	1382	−1362	470	−1632	0.63	0.22	−51	3
		m	6	623	347	1118	−420	388	−1098	2.26	1.04	−37	10
		m/p	12	1930	1261	4016	−1225	888	−2714	1.9	0.59	−29	7
		p	6	2639	1027	3538	−1569	687	−2133	1.76	0.24	−21	1
	All left		30	1723	1221	4016	−1174	793	−2713	1.76	0.75	−32	11
	Right (BS)	a	4	839	135	976	−1181	213	−1419	0.71	0.02	67	2
		a/m	3	1759	300	2064	−2404	399	−2791	0.73	0.01	61	0
		m	19	2017	476	2530	−2757	644	−3405	0.73	0.01	61	1
		m/p	7	1216	742	2311	−1661	1015	−3113	0.74	0.02	61	1
		p	15	1584	650	2379	−2204	908	−3307	0.72	0.02	62	0
	All right		48	1651	655	2530	−2271	894	−3405	0.73	0.01	62	1
	All bites		78	1679	908	4016	−1849	1007	−3405	1.13	0.69	19	43
Left medial splenial	Left (WS)	a/m	4	336	181	532	−724	422	−1131	0.48	0.04	110	4
		m	6	198	85	264	−410	186	−595	0.5	0.08	113	2
		m/p	12	242	132	454	−541	302	−949	0.47	0.07	115	3
		p	8	252	52	332	−552	130	−708	0.46	0.06	113	2
	All left		30	249	116	532	−542	267	−1131	0.47	0.07	114	3
	Right (BS)	a	4	112	26	139	−199	50	−246	0.57	0.04	113	2
		a/m	3	96	29	127	−182	58	−243	0.53	0.01	112	1
		m	19	112	32	196	−179	47	−243	0.68	0.35	103	25
		m/p	7	119	60	232	−243	133	−496	0.5	0.07	112	1
		p	15	156	89	423	−278	155	−735	0.57	0.07	111	2
	All right		48	126	61	423	−221	112	−735	0.6	0.23	109	16
	All bites		78	173	105	532	−345	243	−1131	0.55	0.19	111	13

a, anterior; a/m, anterior/middle; m, middle; m/p, middle/posterior; p. posterior.

Principal strain orientations are axial circular data in which an ε_1 orientation of $0°$ is equal to $180°$ and the zero point is arbitrary. These data cannot be analyzed using traditional statistical methods. Quantitative analyses of *in vivo* principal strain data were performed in ORIANA 3.13 (Kovach Computing Services, Anglesey, UK; www.kovcomp.com). To conduct these analyses, all angle data were converted to positive values, thus $-30°$ was converted to $330°$. Additionally, ORIANA converts all axial data to values between 0 and $180°$. Readers are urged to note these changes when comparing descriptive statistics from Tables 2–7 to circular statistics from Tables 8–10.

Descriptive circular statistics (Tables 8–10) were calculated for ε_1 orientations at each gage site, with data grouped according to broad regions of the mandible (i.e. lateral, medial or ventral surfaces) and whether bites were ipsilateral or contralateral to the gage site (yielding working- and balancing-side bites). The statistics presented here include: the mean angle of the vectors (μ) relative to the reference axis describe above; length of the mean vector (r), ranging from 0 to 1, which is a measure of angular dispersion with values closer to 1 indicating that individual observations are clustered more closely around the mean; the concentration (k), which measures the departure of the distribution from a uniform distribution (or perfect circle); circular variance (V), which is calculated as $V = 1 - r$ and is equivalent to its linear counterpart; the circular standard deviation (S), calculated as $S = [-2\ln(2)]^{1/2}$; the standard error of the mean; and the 95 and 99% confidence intervals derived from standard error. Additionally, Rayleigh's test of uniformity and Watson's U^2 test were used to determine whether data are derived from a von Mises distribution (continuous probability distribution on a circle, not to be confused with von Mises stress). A more detailed review of circular statistics can be found in Zar (1999).

Table 4 Descriptive statistics for principal (ε_1 and ε_2) and $|(\varepsilon_1/\varepsilon_2)|$ strain magnitude and ε_1 orientation for experiment 99.

Gauge location	Bite side	Bite position	n	ε_1 Mean	SD	Max	ε_2 Mean	SD	Max	$\varepsilon_1/\varepsilon_2$ Ratio Mean	SD	ε_1 Orientation Mean	SD
Right dorsolateral dentary	Midline		6	188	83	342	−149	73	−284	1.31	0.39	−2	7
	Left (BS)	m	2	272	3	274	−201	1	−202	1.35	0.01	20	0
		p	1	137		137	−157		−157	0.87		−26	
	All left		3	227	78	342	−186	−26	−202	1.19	0.27	4	27
	Right (WS)	a/m	2	797	583	1210	−618	638	−1069	1.72	0.82	−25	21
		m	7	365	375	1188	−145	185	−554	3.1	0.86	−18	14
		m/p	2	52	9	58	−2	1	−2	54.33	20.53	−22	1
		p	9	382	399	1415	−199	212	−722	2.26	0.8	−32	29
	All right		20	384	399	1415	−202	274	−1069	7.71	19.73	−25	22
	All bites		29	327	342	1415	−190	229	−1069	5071	16.54	−18	23
Right lateral dentary	Midline		6	608	185	966	−589	157	−892	1.02	0.05	16	25
	Left (BS)	a	1	1072		1072	−894		−894	1.2		31	
		m	3	1364	288	1630	−1106	209	−1299	1.23	0.03	30	0
		m/p	4	572	70	676	−444	60	−531	1.29	0.02	29	1
		p	2	756	172	877	−594	145	−697	1.27	0.02	27	2
	All left		10	897	388	1072	−718	322	−1299	1.26	0.04	29	2
	Right (WS)	a/m	2	1381	60	1424	−1531	30	−1553	0.9	0.02	−47	1
		m	7	1229	578	2226	−1192	490	−1779	1.02	0.18	−45	3
		m/p	2	409	110	487	−250	116	−332	1.72	0.36	−45	0
		p	9	944	316	1436	−606	199	−986	1.63	0.63	−50	6
	All right		20	1034	469	2226	−868	501	−1779	1.35	0.54	−48	5
	All bites		36	925	433	2226	−780	422	−1779	1.27	0.42	−6	55
Right ventral dentary	Midline		6	1072	218	1423	−1938	385	−2463	0.55	0.03	97	6
	Left (BS)	a	1	1046		1046	−1712		−1712	0.61		90	
		m	3	1313	277	1560	−2132	459	−2537	0.62	0	90	0
		m/p	4	509	66	604	−813	118	−985	0.63	0.01	90	1
		p	2	832	462	1158	−1453	849	−2053	0.58	0.02	93	4
	All left		10	869	411	1560	−1427	689	−2537	0.61	0.02	91	2
	Right (WS)	a/m	2	960	180	1087	−1711	626	−2153	0.58	0.11	−50	7
		m	7	754	295	1251	−807	320	−1230	1	0.35	−32	16
		m/p	2	428	82	486	−187	43	−217	2.31	0.09	−2	1
		p	9	1922	685	2987	−971	336	−1470	1.97	0.1	4	2
	All right		20	1268	782	2987	−909	478	−2153	1.53	0.63	−15	23
	All bites		36	1124	643	2987	−1224	650	−2537	1.11	0.66	33	57
Right medial splenial	Midline		6	765	131	967	−1398	280	−1847	0.55	0.02	53	6
	Left (BS)	a	1	754		754	−1567		−1567	0.48		−43	
		m	3	920	142	1066	−2139	512	−2606	0.44	0.05	−43	1
		m/p	4	307	61	390	−709	114	−880	0.43	0.04	−47	1
		p	2	632	261	816	−1366	711	−1868	0.48	0.06	−46	3
	All left		10	601	297	1066	−1355	717	−2606	0.45	0.04	−45	2
	Right (WS)	a/m	2	678	483	1019	−1084	686	−1569	0.61	0.06	−80	2
		m	7	386	255	876	−554	255	−1032	0.66	0.13	−70	19
		m/p	2	183	36	209	−272	33	−295	0.67	0.05	−37	1
		p	9	518	468	1693	−547	269	−1181	0.84	0.28	35	32
	All right		20	455	376	1693	−575	337	−1569	0.74	0.22	−38	57
	All bites		36	547	340	1693	−929	605	−2606	0.63	0.21	−31	45

a, anterior; a/m, anterior/middle; m, middle; m/p, middle/posterior; p, posterior.

To determine whether working and balancing sides strain regimes differ, principal strain orientations recorded within the same gage during ipsilateral vs. contralateral biting were compared using a nonparametric Mardia–Watson–Wheeler test (for data that did not match a von Mises distribution) or a parametric Watson–Williams *F*-test (when data matched a von Mises distribution). These tests determine whether two or more distributions are identical; significant differences between distributions lead to a large *W* statistic and low probability of distributions being identical. To determine whether strain orientation changed as load magnitude increased, circular-linear correlation coefficients were calculated between ε_1 orientation and magnitude (Zar, 1999).

Table 5 Descriptive statistics for principal (ε_1 and ε_2) and $|(\varepsilon_1/\varepsilon_2)|$ strain magnitude and ε_1 orientation for experiment 102.

Gauge location	Bite side	Bite position	n	ε_1 Mean	SD	Max	ε_2 Mean	SD	Max	$\varepsilon_1/\varepsilon_2$ Ratio Mean	SD	ε_1 Orientation Mean	SD
Left dorsolateral dentary	Left (WS)	a/m	3	916	470	1450	−560	352	−960	1.71	0.19	−19	5
		m	12	1311	590	2256	−753	335	−1202	1.76	0.14	−23	6
		m/p	2	1290	763	1830	−596	383	−867	2.21	0.14	−26	4
		p	5	1264	570	2244	−565	267	−889	2.39	0.63	−79	12
	All left		22	1245	558	2256	−670	316	−1202	1.94	0.42	−35	25
	Right (BS)	m	5	1056	254	1414	−1127	263	−1472	0.94	0.03	27	2
		m/p	4	1158	413	1642	−1203	419	−1678	0.96	0.04	24	2
		p	5	1372	539	1777	−1379	581	−1742	1.03	0.1	23	2
	All right		14	1198	410	1777	−1239	422	−1742	0.98	0.07	24	2
	All bites		36	1227	500	2256	−891	453	−1742	1.56	0.58	−10	35
Left lateral dentary	Midline		3	844	183	985	−973	151	−1078	0.86	0.06	−39	1
	Left (WS)	a	2	337	70	426	−509	133	−603	0.75	0.06	−35	2
		a/m	9	860	246	1207	−876	293	−1338	1.01	0.15	−39	1
		m	19	1482	696	2728	−1301	636	−2142	1.16	0.13	−38	9
		m/p	6	1231	728	2589	−829	645	−1801	2.15	1.83	−38	4
		p	11	1174	488	2312	−183	198	−629	11.08	8.68	−47	18
	All left		47	1212	628	2728	−864	650	−2142	3.4	5.69	−40	11
	Right (BS)	a	2	836	48	870	−851	24	−868	0.98	0.03	40	0
		a/m	2	1308	159	1420	−1343	202	−1486	0.98	0.03	40	1
		m	8	1457	223	1694	−1525	248	−1800	0.96	0.01	37	1
		m/p	11	1232	389	1855	−1279	449	−2027	0.98	0.07	36	1
		p	13	1336	465	1901	−1413	541	−2072	0.97	0.08	36	2
	All right		36	1302	385	1901	−1362	442	−2072	0.97	0.06	36	2
	All bites		83	1227	532	2728	−1071	608	−2142	2.25	4.34	−4	39
Left ventral dentary	Midline		3	590	24	618	−1066	105	−1142	0.56	0.05	60	1
	Left (WS)	a	2	390	45	422	−383	69	−432	1.03	0.07	−39	1
		a/m	9	296	68	368	−316	60	−454	0.96	0.24	−39	12
		m	19	291	95	413	−420	136	−787	0.72	0.23	−37	13
		m/p	6	188	53	282	−377	119	−558	0.56	0.28	−57	22
		p	11	540	391	1641	−569	375	−1266	1.11	0.56	−81	42
	All left		47	341	228	1641	−428	219	−1266	0.85	0.38	−50	29
	Right (BS)	a	2	330	101	401	−747	98	−816	0.44	0.08	−62	2
		a/m	2	511	174	633	−1127	371	−1390	0.45	0.01	−63	0
		m	8	659	113	829	−1488	281	−1935	0.44	0.02	−68	3
		m/p	11	547	210	924	−1344	545	−2326	0.41	0.03	−65	3
		p	12	598	248	989	−1470	648	−2527	0.41	0.03	−66	3
	All right		35	576	206	989	−1374	526	−2527	0.42	0.03	−66	3
	All bites		82	445	244	1641	−839	595	−2527	0.66	0.35	−47	23
Left ventral splenial	Midline		1	723		723	−1900		−1900	0.38		89	
	Left (WS)	a	2	638	237	805	−1527	531	−1902	0.42	0.01	−82	23
		a/m	6	455	141	615	−966	301	−1366	0.47	0.02	−80	2
		m	7	258	128	407	−365	141	−519	0.69	0.2	−70	15
		m/p	4	375	211	664	−356	232	−668	1.31	0.79	−33	44
		p	4	1482	481	1794	−768	149	−896	1.89	0.42	11	4
	All left		23	576	492	1794	−691	435	−1902	0.93	0.64	−53	39
	Right (BS)	a	2	341	159	454	−994	330	−1228	0.33	0.05	−98	4
		a/m	2	554	319	780	−1709	742	−2234	0.31	0.05	−95	4
		m	3	781	112	907	−2300	357	−2670	0.34	0.01	−92	1
		m/p	7	481	251	812	−1374	778	−2390	0.4	0.19	−105	35
		p	8	662	306	1187	−1773	881	−3454	0.38	0.02	−93	1
	All right		22	581	271	1187	−1641	780	−3454	0.37	0.11	−97	19
	All bites		46	576	391	1794	−1174	783	−3454	0.64	0.54	58	37

Table 5. (continued)

Gauge location	Bite side	Bite position	n	ε_1 Mean	SD	Max	ε_2 Mean	SD	Max	$\varepsilon_1/\varepsilon_2$ Ratio Mean	SD	ε_1 Orientation Mean	SD
Left medial splenial	Midline		3	582	118	698	−839	95	−948	0.69	0.09	148	7
	Left (WS)	a	2	449	160	562	−959	338	−1198	0.47	0	113	1
		a/m	9	512	175	773	−903	363	−1428	0.59	0.09	100	6
		m	19	654	319	1070	−927	451	−1549	0.71	0.1	93	9
		m/p	6	577	250	950	−560	382	−1177	1.33	0.78	72	27
		p	11	956	252	1401	−363	144	−608	2.86	0.79	40	9
	All left		47	679	306	1401	−745	431	−1549	1.26	1.03	80	27
	Right (BS)	a	2	514	39	541	−548	27	−567	0.94	0.12	−15	5
		a/m	2	764	49	798	−837	145	−939	0.92	0.1	−17	4
		m	8	810	109	905	−903	131	−1027	0.9	0.03	−15	1
		m/p	11	666	192	966	−757	267	−1218	0.9	0.08	−15	3
		p	12	733	231	1010	−825	329	−1246	0.97	0.19	−14	7
	All right		35	71	190	1010	−806	260	−1246	0.93	0.14	−15	5
	All bites		82	688	259	1401	−770	360	−1549	1.1	0.78	41	53

a, anterior; a/m, anterior/middle; m, middle; m/p, middle/posterior; p, posterior.

Lastly, two-way ANOVAS were carried out using the Circular Statistics Toolbox for MATLAB (Berens, 2009) to determine whether differences in ε_1 orientations from gage sites located in dorsolateral, lateral, ventral and medial areas of the jaw across all experiments were due to changes in bite point or individual variation (Table 11).

All statistical tests discussed below were conducted using SPSS v11.5 (SPSS Inc., Chicago, IL). Shear strain data were averaged across *in vivo* experiments (and not sorted into different bite point locations for this analysis); summarized results for the entire mandible and for the dentary and splenial bones are indicated in Table 12. To quantitatively evaluate the degree of variation in strain orientation with changes in bite point, ANOVAS were performed to assess whether significant differences in ε_1 orientation existed among bite points for individual gages during all experiments (Table 13).

Results

Principal strain (ε_1) orientations: lateral mandible

In vivo strain orientations
During biting ipsilateral to the gages (i.e. in the working side mandible) ε_1 strains on the lateral aspect of the mandible (dorsolateral and lateral gages) are oriented anteroinferiorly, between −12 and −79° from the reference axis (Fig. 2, Tables 3–6). The only exception is the lateral gage in Experiment 103, which exhibits ε_1 strains oriented anterosuperiorly at an angle of approximately 30°. With the exception of Experiment 75, ε_1 strain orientations tend to rotate clockwise as the bite point moves posteriorly.

During biting contralateral to the gage site (i.e. in the balancing side mandible) (Fig. 3, Tables 3–6), ε_1 is oriented anterosuperiorly between 23 and 40° from the reference axis. Exceptions include the dorsolateral gage in Experiment

99 (ε_1 orientations ranging from 20 to −26°) and, as during ipsilateral biting, the lateral gage in Experiment 103 in which ε_1 is oriented posterosuperiorly. Contralateral biting does not produce any observable trends of changes in ε_1 orientation with changes in bite point. Mean vector length and concentration (Table 8) reveal that ε_1 strains are more concentrated (i.e. orientations are less variable) during contralateral than ipsilateral biting.

In all experiments, Mardia–Watson–Wheeler and Wheeler–Williams tests show that lateral gage ε_1 orientations during ipsilateral bites are significantly different from those recorded during contralateral biting (Table 8). Two-way ANOVA (Table 11) suggests that bite point has a significant impact on ε_1 orientations in lateral gages (ipsilateral and contralateral biting) and dorsolateral gages (ipsilateral biting) but not in dorsolateral gages during contralateral bites. Additionally, analyses reveal significant differences in ε_1 orientation between similarly located gages (dorsolateral and lateral gages) in different experiments when both biting side and bite point are taken into account (Table 11); this may be due to slight differences in gage location between experiments or individual differences between research subjects. For most dorsolateral and lateral gage sites, strain orientation appears to be strongly correlated with strain magnitude (Table 8), although these comparisons are rarely statistically significant.

FEM strain orientations
Working side strain orientations at dorsolateral gages are directed horizontally to anteroinferiorly, ranging from +1 to −83° (Fig. 2, Table 7). At working side lateral gage locations, orientations range from superior (90°) to anteroinferior (−78°). ε_1 orientations tend to rotate clockwise

Table 6 Descriptive statistics for principal (ϵ_1 and ϵ_2) and $|(\epsilon_1/\epsilon_2)|$ strain magnitude and ϵ_1 orientation for experiment 103.

Gauge location	Bite side	Bite position	n	ϵ_1			ϵ_2			ϵ_1/ϵ_2 Ratio		ϵ_1 Orientation	
				Mean	SD	Max	Mean	SD	Max	Mean	SD	Mean	SD
Right dorsolateral dentary	Left (BS)	a/m	6	1334	282	1751	−1141	246	−1489	1.17	0.03	38	2
		m	3	1380	248	1606	−1176	179	−1335	1.17	0.03	37	1
		m/p	6	859	435	1430	−655	372	−1115	1.38	0.17	37	3
		p	4	1021	188	1301	−817	147	−1021	1.25	0.06	37	2
	All left		19	1125	373	1751	−925	340	−1489	1.25	0.13	37	3
	Right (WS)	a/m	3	1411	81	1503	−1122	148	−1254	1.27	0.12	−12	5
		m	1	874		874	−593		−593	1.47		−14	
		m/p	4	1257	570	1825	−113	651	−170	24.99	34.79	−58	22
		p	3	2506	128	2651	−285	8	−292	8.79	0.7	−78	2
	All right		11	1605	677	2651	−479	442	−1254	11.96	21.89	−47	31
	All bites		30	1301	547	2651	−761	432	−1489	5.18	13.89	6	45
Right lateral dentary	Left (BS)	a/m	6	1385	249	1775	−1588	328	−2039	0.88	0.06	115	1
		m	9	1597	231	1858	−1821	260	−2129	0.88	0.01	114	1
		m/p	6	823	364	1248	−827	484	−1426	1.11	0.28	108	7
		p	9	1155	441	1911	−1267	530	−2170	0.92	0.06	113	2
	All left		30	1267	428	1911	−1409	539	−2170	0.94	0.15	113	4
	Right (WS)	a/m	9	1720	604	2958	−1489	157	−1727	1.15	0.38	31	2
		m	3	2018	842	2835	−840	731	−1511	16.29	25.98	35	5
		m/p	4	1870	670	2709	−328	258	−648	10.53	8.83	31	5
		p	8	2088	281	2417	−112	75	−265	49.39	84.26	32	4
	All right		24	1905	546	2958	−755	673	−1727	20.69	51.83	32	4
	All bites		54	1551	576	2958	−1119	681	−2170	9.72	35.55	77	50
Right ventral dentary	Left (BS)	a/m	6	846	164	1087	−822	181	−1045	1.04	0.07	103	3
		m	9	882	91	963	−799	67	−896	1.1	0.07	103	0
		m/p	6	486	255	790	−470	282	−821	1.1	0.14	97	9
		p	9	662	218	1041	−617	187	−946	1.07	0.04	103	2
	All left		30	730	234	1087	−683	222	−1045	1.08	0.08	102	5
	Right (WS)	a/m	9	657	150	843	−1007	346	−1398	0.69	0.15	−21	14
		m	3	687	444	1193	−655	146	−816	0.99	0.42	3	31
		m/p	4	623	266	880	−317	174	−499	2.33	1.28	26	9
		p	8	974	242	1331	−572	151	−829	1.72	0.26	36	2
	All right		24	761	276	1331	−703	350	−1398	1.35	0.81	7	29
	All bites		54	743	252	1331	−692	283	−1398	1.2	0.55	60	47
Right medial splenial	Left (BS)	a/m	6	861	187	1097	−2108	532	−2806	0.41	0.03	99	0
		m	7	1018	159	1176	−2500	383	−2828	0.41	0.03	100	1
		m/p	6	662	275	1055	−1326	792	−2445	0.57	0.15	99	1
		p	8	788	334	1512	−1735	757	−3436	0.45	0.03	99	1
	All left		27	833	273	1512	−1926	744	−3436	0.46	0.1	99	1
	Right (WS)	a/m	7	651	397	1534	−465	176	−733	1.44	0.62	74	12
		m	1	432		432	−426		−426	0.01		94	
		m/p	4	724	476	1176	−998	481	−1321	0.68	0.21	−23	78
		p	3	2084	701	2565	−1743	121	−1878	1.22	0.47	−7	2
	All right		15	942	735	2565	−860	574	−1878	1.16	0.56	35	49
	All bites		42	872	484	2565	−1545	855	−3436	0.71	0.48	67	43

a, anterior; a/m, anterior/middle; m, middle; m/p, middle/posterior; p, posterior.

as bite point moves posteriorly, although there is no clear trend for FEM gage site 4, corresponding to the lateral gage of Experiment 75. Strain orientations on the lateral side of the mandible vary with gage location and bite point, as seen in FEM strain fields (strain fields are close-up views of the FEM with vectors illustrating ϵ_1 orientation for each element) (Fig. 4). During anterior and middle bites, ϵ_1 is oriented anteroinferiorly at all lateral gage sites; however, during posterior biting (when the bite point is immediately superior to the gages) there are strong local variations in strain orientation.

On the balancing side (Fig. 3, Table 7), ϵ_1 orientations are directed horizontally to anteroinferiorly for dorsolateral gages (ranging from 1 to −55°) but anterosuperiorly (from
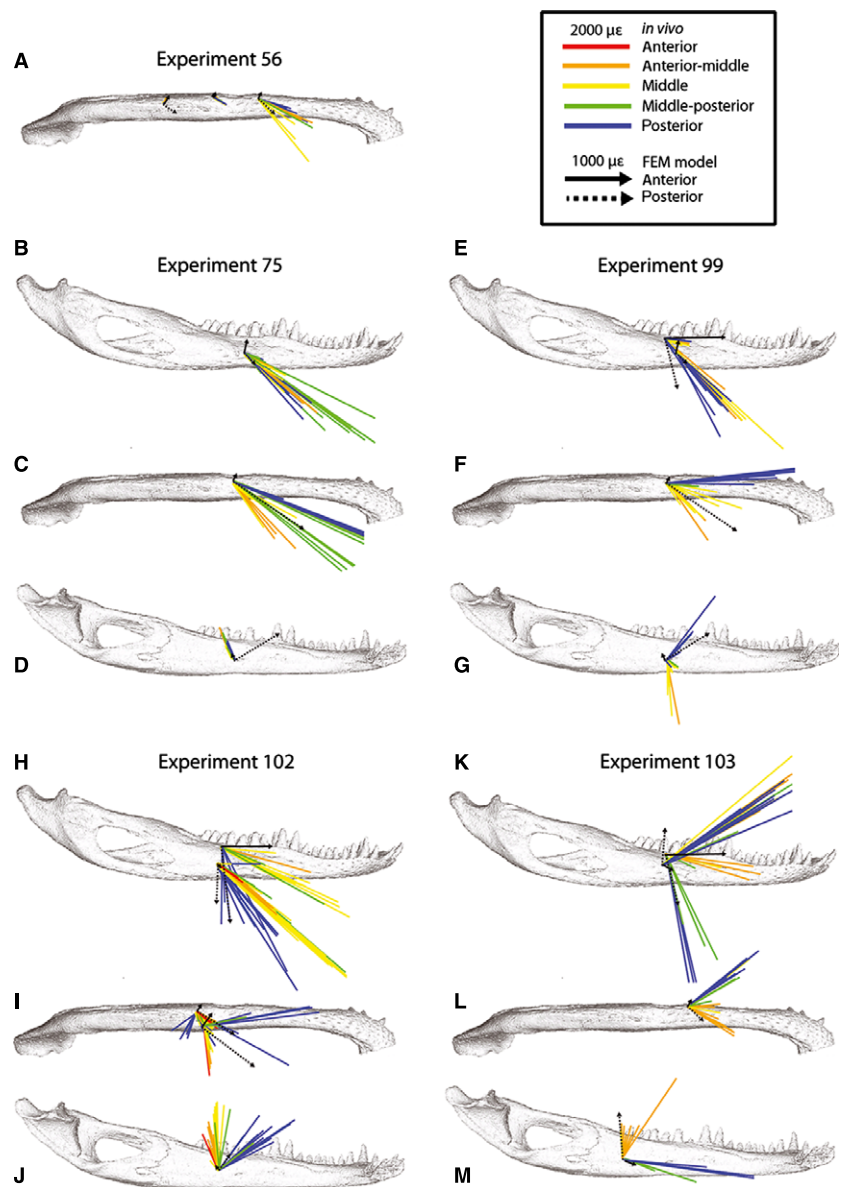
Fig. 2 Orientations of maximum principal strain (ε_1) on the working side mandible. Colored arrows represent variations in bite point in *in vivo* experiments (see inset for color key); strain orientation for every recorded bite during experiments is shown for every gage site in five experiments for lateral (B,E,H,K), ventral (A,C,F,I,L) and medial (D,G,J,M) views. Black arrows represent strain orientations during anterior (solid line) and posterior bites (broken line) in the FEM (finite element model) in areas corresponding to *in vivo* gage sites. Note difference in scale between *in vivo* and FEM strain in the inset.

29 to 38°) for lateral gages. ε_1 orientations rotate clockwise as bite point moves posteriorly; however, ε_1 orientation does not vary by more than 5° within any balancing side dorsolateral or lateral gage site. Strain fields (Fig. 4) reveal that the strain orientations on the lateral aspect of the balancing side remain similar across gage sites.

Strain orientations within dorsolateral and lateral gages vary less with changes in bite point on the balancing side (Fig. 3) than on the working side of the FEM (Figs 2 and 4). The range of strain orientations predicted by the FEM overlapped the range of *in vivo* ε_1 orientations recorded in dorsolateral gages (Experiments 99, 102, 103) during ipsilateral biting, lateral gages (Experiments 75, 99, 102) during ipsilateral and contralateral biting, and the lateral gage of Experiment 103 during ipsilateral biting. In contrast, FEM strain orientations did not match

in vivo orientations at dorsolateral gages during contralateral biting, and were nearly perpendicular to ε_1 orientations recorded at the lateral gage of Experiment 103 during contralateral biting; in this context, it should be observed that the strain orientations recorded during Experiment 103 are anomalous.

Principal strain (ε_1) orientations: medial mandible

In vivo strain orientations
In vivo strain orientations recorded on the medial aspect of the mandible during ipsilateral biting (Fig. 2, Tables 3–6) are highly variable both within and between experiments, and it is difficult to make generalizations regarding the strain orientations for this region. In contrast, during contralateral biting, ε_1 on the medial aspect of the mandible is con-
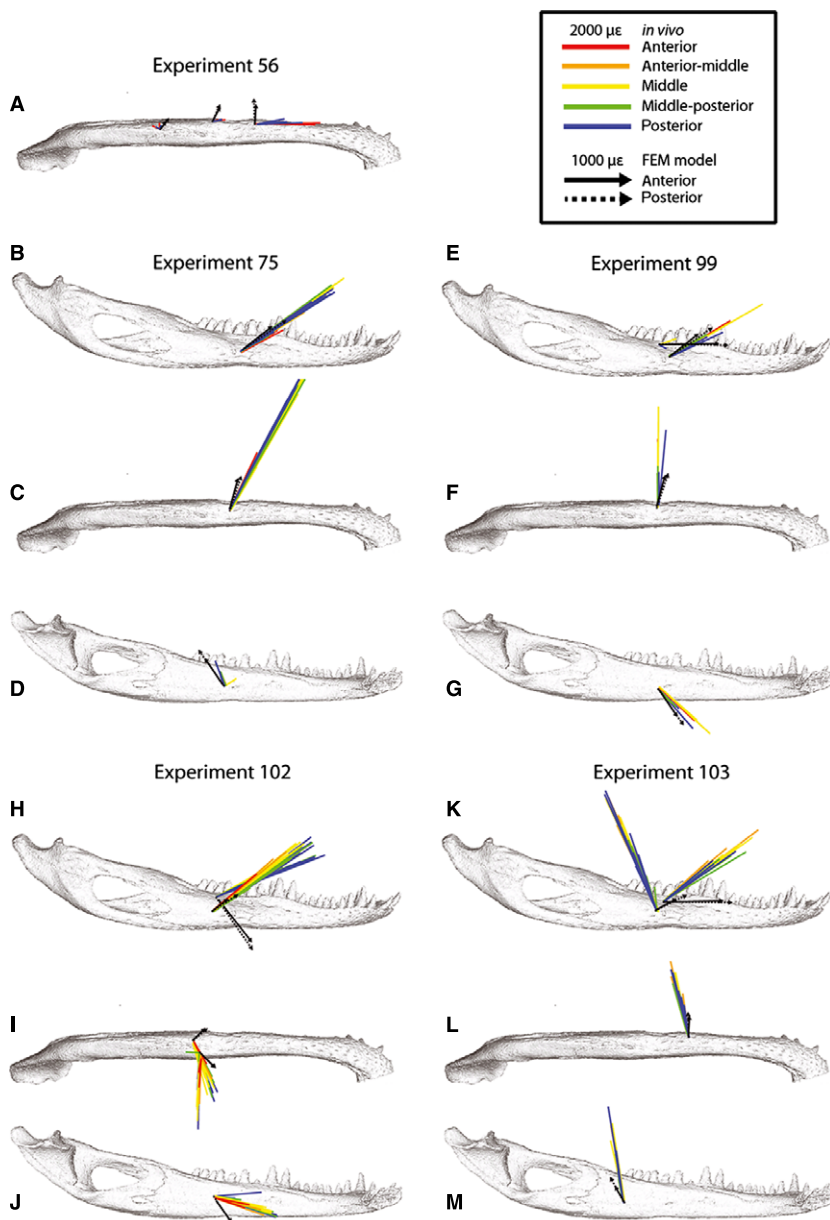
Fig. 3 Orientations of maximum principal strain (ε_1) on the balancing side mandible. Colored arrows represent variations in bite point in *in vivo* experiments (see inset for color key); strain orientation for every recorded bite during experiments is shown for every gage site in five experiments for lateral (B,E,H,K), ventral (A,C,F,I,L) and medial (D,G,J,M) views. Black arrows represent strain orientations during anterior (solid line) and posterior bites (broken line) in the FEM (finite element model) in areas corresponding to *in vivo* gage sites. Note difference in scale between *in vivo* and FEM strain in the inset.

sistently oriented anteroinferiorly from the reference axis (Fig. 3; Tables 3–6) with values ranging from −14 to −81°. Neither ipsilateral nor contralateral biting produce any observable trends of changes in ε_1 orientation with changes in bite point. As with lateral gages, ε_1 strains on the medial aspect of the mandible are more concentrated during contralateral biting than during ipsilateral biting (Table 9).

In all experiments, medial ε_1 orientations during ipsilateral bites are significantly different from those recorded during contralateral biting (Table 9). Two-way ANOVA (Table 11) suggests that differences in gage site/research subject across experiments has a significant impact on medial ε_1 orientations (ipsilateral and contralateral biting) and that bite point has a significant impact on medial ε_1 orien-

tations during ipsilateral biting but not during contralateral biting. Circular-linear correlations do not reveal strong relationships between strain orientation and magnitude at most medial gage sites (Table 9).

FEM strain orientations
Strain orientations on the medial working side of the FEM were directed anterosuperiorly to anteroinferiorly, ranging from 32 to −86° (Fig. 2, Table 7). On the balancing side (Fig. 3, Table 7), ε_1 orientations were directed anteroinferiorly, ranging from −54 to −63°, and varied by no more 4° within any individual gage site, again demonstrating that strain orientations varied less with changes in bite point on the balancing side than on the working side of the FEM.

Table 7 Descriptive statistics for principal (ε_1 and ε_2) and $|(\varepsilon_1/\varepsilon_2)|$ strain magnitude and ε_1 orientation for the gage sites in the FEM. Maximum and mean values as well as standard deviations are based on results from bricks within gage sites.

Gage ID	Gage side	No. of bricks	Bite position*	E1 Mean	SD	Max	E2 Mean	SD	Max	E1 orientation Mean	SD	E1/E2 ratio Mean	SD
1 Ventral anterior dentary	Right (WS)	24	a	61	8	71	−291	28	−342	64	2	0.21	0.02
			a/m	63	4	72	−226	10	−243	74	2	0.28	0.02
			m	57	8	73	−77	19	−115	−84	8	0.81	0.3
			m/p	136	44	213	−37	16	−61	−51	9	5.21	6.19
			p	176	41	248	−37	14	−59	−43	3	6	6
	Left (BS)	25	a	162	24	199	−436	52	−570	87	4	0.37	0.05
			a/m	187	27	228	−451	52	−587	90	4	0.42	0.05
			m	199	29	242	−456	51	−591	91	4	0.44	0.06
			m/p	204	29	248	−458	51	−592	91	4	0.45	0.06
			p	203	29	246	−444	47	−569	92	4	0.46	0.06
2 Ventral posterior dentary	Right (WS)	21	a	50	9	68	−305	37	−357	71	2	0.16	0.02
			a/m	54	8	74	−380	31	−327	77	2	0.19	0.02
			m	44	5	54	−160	13	−192	80	2	0.28	0.04
			m/p	43	8	59	−74	11	−103	88	4	0.59	0.11
			p	0	0	0	2	0	2	−5	7	0	0
	Left (BS)	24	a	133	20	183	−505	57	−633	62	2	0.26	0.03
			a/m	147	21	201	−512	56	−634	63	2	0.29	0.03
			m	153	22	211	−509	56	−628	64	2	0.3	0.03
			m/p	155	22	215	−506	55	−623	65	3	0.31	0.03
			p	152	22	214	−481	54	−594	66	3	0.32	0.04
3 Ventral angular	Right (WS)	18	a	83	20	126	−473	76	−561	61	5	0.18	0.05
			a/m	74	12	98	−443	66	−525	57	6	0.17	0.04
			m	32	10	54	−309	51	−374	56	6	0.1	0.04
			m/p	11	7	23	−224	46	−279	57	4	0.05	0.03
			p	126	82	289	−112	30	−177	−33	9	1.27	0.13
	Left (BS)	21	a	117	29	169	−621	143	−853	53	4	0.2	0.04
			a/m	116	32	177	−611	151	−859	52	4	0.19	0.05
			m	106	36	174	−584	160	−846	52	4	0.18	0.05
			m/p	99	37	170	−567	165	−836	53	5	0.18	0.05
			p	84	36	154	−528	172	−795	55	5	0.16	0.05
4 Lateral dentary	Right (WS)	21	a	116	55	203	−88	25	−154	79	14	1.55	0.92
			a/m	130	33	188	−158	37	−229	90	8	0.9	0.39
			m	58	7	74	−231	37	−288	−68	3	0.25	0.05
			m/p	64	10	81	−327	52	−404	−57	5	0.2	0.03
			p	128	27	188	−322	84	−459	−44	4	0.41	0.11
	Left (BS)	23	a	289	96	426	−205	39	−293	38	8	1.47	0.51
			a/m	349	74	490	−226	45	−330	37	7	1.61	0.52
			m	387	77	532	−234	49	−347	36	7	1.73	0.54
			m/p	403	79	550	−237	51	−354	35	7	1.78	0.55
			p	414	78	560	−229	51	−348	34	6	1.9	0.58
5 Ventral dentary	Right (WS)	22	a	65	10	84	−738	68	−900	64	3	0.09	0.01
			a/m	53	12	78	−571	51	−709	74	3	0.09	0.02
			m	98	34	167	−200	23	−263	−80	5	0.5	0.19
			m/p	342	93	565	−102	23	−165	−50	3	3.39	0.74
			p	674	92	938	−103	19	−142	−34	3	7	0.72
	Left (BS)	21	a	253	19	288	−838	118	−1051	75	3	0.31	0.04
			a/m	282	20	322	−847	121	−1067	74	3	0.34	0.05
			m	295	21	337	−843	121	−1066	73	3	0.36	0.05
			m/p	299	22	343	−839	121	−1062	73	3	0.36	0.05
			p	291	22	335	−795	115	−1010	72	3	0.37	0.05

Table 7. (continued)

Gage ID	Gage side	No. of bricks	Bite position*	E1			E2			E1 orientation		E1/E2 ratio	
				Mean	SD	Max	Mean	SD	Max	Mean	SD	Mean	SD
6 Medial splenial	Right (WS)	24	a	63	14	89	−277	32	−334	116	8	0.23	0.05
			a/m	63	15	97	−179	20	−220	122	9	0.35	0.09
			m	190	19	225	−140	12	−167	142	2	1.43	0.17
			m/p	312	27	388	−135	33	−181	147	3	2.49	0.77
			p	420	55	544	−30	18	−80	32	7	30.68	51.32
	Left (BS)	23	a	255	37	322	−628	48	−700	124	2	0.41	0.08
			a/m	295	41	370	−683	53	−765	125	2	0.44	0.08
			m	321	43	401	−721	57	−808	125	2	0.45	0.08
			m/p	333	45	416	−738	58	−828	125	2	0.46	0.08
			p	351	46	438	−751	60	−844	125	2	0.47	0.09
7 DL dentary	Right (WS)	25	a	490	64	626	−56	18	−93	1	3	9.38	2.37
			a/m	396	47	496	−45	16	−81	−6	4	9.66	3.47
			m	112	11	128	−44	10	−74	−28	8	2.64	0.62
			m/p	40	17	70	−158	26	−214	−68	2	0.26	0.11
			p	412	91	543	−707	122	−1000	−76	5	0.61	0.2
	Left (BS)	18	a	472	109	556	−146	30	−192	1	4	3.25	0.93
			a/m	503	111	581	−166	36	−221	0	3	3.06	0.84
			m	527	117	610	−183	37	−241	0	3	2.93	0.84
			m/p	539	119	625	−191	38	−251	0	3	2.87	0.82
			p	547	121	634	−201	36	−262	−1	4	2.77	0.82
8 DL dentary	Right (WS)	23	a	401	53	492	−34	11	−56	0	2	12.96	4.4
			a/m	357	47	434	−16	10	−40	−6	3	47	64
			m	149	20	181	−6	3	−12	−18	8	41	31
			m/p	57	13	80	−32	13	−56	−57	7	2.12	1.12
			p	615	66	720	−599	107	−786	−83	3	1.06	0.23
	Left (BS)	22	a	426	50	508	−140	18	−180	−52	1	3.09	0.57
			a/m	451	51	534	−165	21	−212	−54	1	2.78	0.51
			m	477	51	559	−183	23	−233	−55	1	2.66	0.46
			m/p	491	51	573	−192	24	−244	−55	1	2.6	0.45
			p	508	50	586	−200	25	−253	−55	2	2.58	0.42
9 Lateral dentary	Right (WS)	24	a	44	26	100	−63	14	−93	−46	11	0.74	0.43
			a/m	89	27	144	−105	16	−140	−50	6	0.88	0.32
			m	82	14	108	−118	15	−146	−62	3	0.72	0.19
			m/p	89	11	108	−137	11	−154	−70	1	0.66	0.12
			p	307	61	414	−47	29	−105	−92	3	22	55
	Left (BS)	20	a	156	25	192	−180	15	−211	38	5	0.87	0.14
			a/m	187	27	225	−206	17	−244	37	4	0.91	0.13
			m	212	28	255	−217	19	−261	35	4	0.98	0.13
			m/p	226	29	270	−222	20	−268	34	3	1.02	0.13
			p	245	31	292	−220	21	−268	33	3	1.12	0.14
10 Ventral dentary	Right (WS)	21	a	69	9	86	−464	43	−566	58	2	0.15	0.02
			a/m	55	6	65	−409	35	−495	62	2	0.13	0.02
			m	27	4	34	−214	18	−249	67	2	0.13	0.02
			m/p	21	9	46	−84	15	−113	86	9	0.26	0.12
			p	350	38	439	−40	11	−58	−32	2	9.54	4.06
	Left (BS)	23	a	142	10	158	−613	64	−711	45	1	0.23	0.02
			a/m	149	10	165	−612	65	−716	43	1	0.25	0.02
			m	152	10	169	−606	67	−714	42	1	0.25	0.03
			m/p	153	10	171	−601	67	−712	42	1	0.26	0.03
			p	149	10	167	−572	66	−680	41	2	0.26	0.03

Table 7. (continued)

Gage ID	Gage side	No. of bricks	Bite position*	E1 Mean	E1 SD	E1 Max	E2 Mean	E2 SD	E2 Max	E1 orientation Mean	E1 orientation SD	E1/E2 ratio Mean	E1/E2 ratio SD
11 Ventral splenial	Right (WS)	22	a	133	12	156	−593	33	−637	55	2	0.22	0.02
			a/m	111	14	138	−474	28	−512	57	3	0.23	0.03
			m	49	9	67	−187	20	−216	59	3	0.27	0.07
			m/p	26	13	60	−8	5	−16	−60	20	6.13	6.96
			p	524	29	569	−127	15	−158	−37	2	4.16	0.46
	Left (BS)	22	a	169	17	201	−789	82	−922	−46	2	0.21	0.02
			a/m	175	19	210	−806	82	−942	−45	2	0.22	0.02
			m	179	20	217	−822	81	−956	−44	2	0.22	0.02
			m/p	181	20	219	−829	80	−962	−44	2	0.22	0.02
			p	179	19	217	−822	77	−948	−45	2	0.22	0.02
12 Medial splenial	Right (WS)	22	a	37	24	87	−77	28	−132	−50	14	0.59	0.5
			a/m	62	32	127	−46	16	−77	−32	12	1.58	1.03
			m	174	15	202	−86	9	−102	−36	3	2.08	0.27
			m/p	257	20	295	−116	8	−130	−38	1	2.21	0.13
			p	157	NA	157	−6	NA	−6	55	NA	24.31	NA
	Left (BS)	20	a	212	25	259	−298	64	−445	−54	3	0.75	0.22
			a/m	246	25	293	−340	68	−493	−55	3	0.76	0.2
			m	269	26	315	−369	72	−527	−55	2	0.76	0.19
			m/p	281	26	327	−383	73	−542	−56	2	0.76	0.18
			p	299	26	344	−398	74	−555	−56	2	0.78	0.18
13 Lateral dentary	Right (WS)	25	a	105	33	184	−56	9	−83	−30	6	1.89	0.6
			a/m	129	25	196	−82	10	−112	−40	4	1.62	0.43
			m	78	9	98	−86	8	−98	−62	2	0.93	0.15
			m/p	79	6	94	−122	14	−159	−78	2	0.66	0.08
			p	300	54	410	−178	44	−281	86	2	1.74	0.32
	Left (BS)	24	a	192	24	237	−167	24	−227	29	6	1.18	0.27
			a/m	226	24	267	−197	25	−262	29	5	1.17	0.23
			m	252	25	296	−211	24	−278	28	5	1.21	0.21
			m/p	265	26	308	−218	24	−285	28	5	1.23	0.21
			p	279	26	324	−217	23	−281	27	4	1.3	0.21
14 Medial splenial	Right (WS)	22	a	96	35	173	−127	35	−202	−21	5	0.75	0.16
			a/m	97	35	177	−89	27	−149	−16	7	1.1	0.27
			m	80	13	106	−17	5	−24	−67	12	5.27	3.31
			m/p	166	14	190	−63	20	−92	96	2	3.02	1.43
			p	378	47	463	−58	26	−115	94	4	8.46	5.09
	Left (BS)	25	a	153	25	207	−244	38	−314	121	2	0.63	0.07
			a/m	169	23	218	−277	39	−349	118	2	0.62	0.07
			m	186	23	236	−310	40	−387	118	2	0.6	0.07
			m/p	196	23	247	−328	41	−406	117	2	0.6	0.07
			p	216	26	271	−358	42	−439	118	2	0.61	0.06

a, anterior; a/m, anterior/middle; m, middle; m/p, middle/posterior; posterior.

Strain fields of the medial aspect of the mandible (Fig. 4) reveal strong local variations in principal strain on the working side during posterior biting.

Despite (or because of) the high variability of ε_1 orientations recorded at medial gages *in vivo* (especially during ipsilateral biting), strain orientations predicted by the FEM overlapped the range of *in vivo* ε_1 orientations during ipsilateral biting (Experiments 75, 102, 103) and contralateral biting (Experiment 99), and were similar to ε_1 orientations recorded during contralateral biting in Experiments 75, 102 and 103.

FEM strain orientations did not fall within the range of data recorded at the medial gage site in Experiment 99 during ipsilateral biting, despite the fact that *in vivo* ε_1 orientations at this site were highly variable (spanning over 115°).

Principal strain (ε_1) orientations: ventral mandible

In vivo strain orientations
On the ventral aspect of the working side, ε_1 strain orientation is highly variable between experiments and gage sites

Table 8 Circular statistics for bone strains from the lateral aspect of the *Alligator* mandible.

Experiment and site	75 Lateral		99 Dorsolateral		99 Lateral		102 Dorsolateral		102 Lateral		103 Dorsolateral		103 Lateral	
Side	WS	BS	WS	BS	WS	BS	WS	BS	WS	BS	WS	BS	WS	BS
Number of observations	30	48	20	3	20	10	22	14	47	36	11	19	24	30
Mean vector (μ)	144.069°	33.141°	155.701°	6.261°	132.284°	29.262°	149.608°	24.43°	139.897°	36.422°	131.333°	37.258°	31.668°	112.724°
Length of mean vector (r)	0.951	0.998	0.741	0.735	0.987	0.998	0.701	0.997	0.939	0.998	0.519	0.996	0.992	0.991
Median	142.955°	33.27°	160.485°	19.41°	133.62°	29.78°	155.08°	24.715°	140.54°	36.61°	116.3°	37.07°	31.765°	114.12°
Concentration	10.447	232.382	2.29	0.599	39.876	238.592	2.014	137.099	8.411	228.833	1.058	138.932	61.425	56.314
Circular variance	0.025	0.001	0.13	0.132	0.006	7.57E-04	0.149	0.001	0.031	0.001	0.241	0.002	0.004	0.004
Circular standard deviation	9.093°	1.881°	22.183°	22.475°	4.566°	1.577°	24.14°	2.187°	10.203°	1.896°	32.815°	2.435°	3.67°	3.835°
Standard error of mean	1.659°	0.272°	4.918°	24.932°	1.021°	0.587°	5.14°	0.655°	1.487°	0.316°	11.655°	0.559°	0.749°	0.7°
95% Confidence interval	140.816°	32.608°	146.06°	317.384°	130.282°	28.112°	139.531°	23.146°	136.982°	35.802°	108.484°	36.163°	30.199°	111.351°
(−/+) for μ	147.322°	33.673°	165.341°	55.138°	134.285°	30.413°	159.685°	25.714°	142.813°	37.041°	154.181°	38.353°	33.137°	114.096°
99% Confidence interval	139.794°	32.441°	143.032°	302.031°	129.654°	27.75°	136.365°	22.743°	136.066°	35.608°	101.307°	35.819°	29.738°	110.92°
(−/+) for μ	148.344°	33.84°	168.37°	70.491°	134.914°	30.774°	162.851°	26.117°	143.729°	37.236°	161.358°	38.697°	33.598°	114.527°
Rayleigh test (Z)	27.125	47.793	10.981	1.621	19.498	9.97	10.816	13.919	41.401	35.843	2.962	18.863	23.609	29.467
Rayleigh test (P)	1.43E-11	< 1E-12	2.82E-06	0.211	1.21E-08	< 1E-12	4.40E-06	7.56E-07	< 1E-12	< 1E-12	0.048	2.13E-08	3.88E-10	2.13E-12
Watson's U² test (U²)	0.071	0.064	0.133	*	0.066	0.095	0.441	0.065	0.657	0.12	0.143	0.061	0.05	0.409
(P)	0.25 > P > 0.15	0.5 > P > 0.25	< 0.025	*	0.5 > P > 0.25	0.15 > P > 0.1	< 0.005	0.5 > P > 0.25	< 0.005	< 0.05	< 0.005	0.5 > P > 0.25	0.5 > P > 0.25	< 0.005
Test for WS/BS differences														
W	58.415		*		20.593		27.174		65.586		21.928		43.03	
P	< 1E-12		*		3.38E-05		1.26E-06		< 1E-12		1.73E-05		4.53E-10	
Circular-linear correlation														
r	0.753	0.789	0.628	*	0.626	0.887	0.865	0.769	0.673	0.568	0.779	0.548	0.414	0.633
P	0.096	0.334	0.251	*	0.149	0.751	0.371	0.329	0.143	0.185	0.004	0.007	0.026	1.06E-05

*Indicates a result could not be calculated.

Table 9 Circular statistics for bone strains from the medial aspect of the *Alligator* mandible.

Experiment and site Side	75 Medial		99 Medial		102 Medial		103 Medial	
	WS	BS	WS	BS	WS	BS	WS	BS
No. of observations	30	48	20	10	47	35	15	27
Mean vector (μ)	113.66°	111.33°	86.855°	134.901°	84.21°	165.116°	99.913°	99.373°
Length of mean vector (*r*)	0.994	0.918	0.302	0.997	0.634	0.988	0.064	0.999
Median	112.99°	111.335°	95.02°	135.22°	92.36°	164.04°	93.55°	99.26°
Concentration	90.202	6.401	0.634	109.854	1.655	43.003	0	879.798
Circular variance	0.003	0.041	0.349	0.002	0.183	0.006	0.468	2.84E-04
Circular standard deviation	3.025°	11.829°	44.322°	2.326°	27.362°	4.394°	67.173°	0.966°
Standard error of mean	0.552°	1.705°	14.636°	0.866°	4.08°	0.743°	*	0.186°
95% Confidence interval	112.577°	107.987°	58.163°	133.204°	76.21°	163.66°	*	99.009°
(−/+) for μ	114.743°	114.673°	115.548°	136.598°	92.209°	166.572°	*	99.738°
99% Confidence interval	112.237°	106.936°	49.15°	132.671°	73.698°	163.203°	*	98.894°
(−/+) for μ	115.083°	115.724°	124.561°	137.132°	94.721°	167.03°	*	99.852°
Rayleigh test (*Z*)	29.667	40.475	1.826	9.934	18.876	34.186	0.061	26.969
Rayleigh test (*P*)	1.81E-12	< 1E-12	0.162	< 1E-12	2.35E-09	< 1E-12	0.942	2.09E-11
Watson's U^2 test (U^2)	0.15	2.292	0.112	0.048	0.556	0.361	*	0.186
Watson's U^2 test (*P*)	< 0.025	< 0.005	< 0.005	> 0.5	< 0.005	< 0.005	*	< 0.005
Test for WS/BS differences								
W	8.422		12.759		64.427		5.66E-04	
P	0.015		1.00E-03		< 1E-12		9.81E-01	
Circular-linear correlation								
r	0.559	0.593	0.698	0.998	0.462	0.700	0.972	0.668
P	0.378	0.454	0.080	0.537	0.271	0.091	0.349	0.244

*Indicates a result could not be calculated.

(Fig. 2, Tables 2–6), directed anteromedially [Experiments 56 (anterior and posterior dentary gages), 75, 99, and 102 (ventral splenial gage)] or anterolaterally [Experiments 56 (angular gage), 102 (ventral dentary gage), and 103]. During ipsilateral biting, ε_1 orientations at ventral gage sites tend to rotate in a counterclockwise direction (relative to the reference axis) as bite point moves posteriorly.

With the exception of Experiment 56, ε_1 on the ventral aspect of the mandible during contralateral biting is nearly perpendicular to the reference axis (Fig. 3, Tables 2–6). In Experiment 56, principal strains are parallel to the reference axis. Contralateral biting does not produce any obvious trend of change in ε_1 orientation with change in bite point. At most ventral gage sites, ε_1 strains are more concentrated during contralateral than ipsilateral biting (Table 10). The exceptions are the posterior dentary and angular gages of Experiment 56, in which the reverse is true.

In all experiments, ventral ε_1 orientations during ipsilateral bites are significantly different from those recorded during contralateral biting (Table 10). Two-way ANOVA (Table 11) suggests that differences in bite point and gage sites/experimental animals have a significant impact on ε_1 orientations. There appears to be some correlation between strain orientation and magnitude at ventral gage sites but these are rarely significant (Table 10).

FEM strain orientations

Working side strain orientations at all ventral gage sites are directed anterolaterally during anterior bites to anteromedially during posterior bites (Fig. 2, Table 7). On the balancing side (Fig. 3, Table 7) ε_1 orientations are directed perpendicular to the reference axis at more anterior gage sites [Experiments 56 (anterior dentary), 75, 99 and 103] but anterolaterally or anteromedially at more posterior gage sites [Experiments 56 (posterior dentary and angular sites) and 102]. Within balancing side gage sites, ε_1 orientations varied by no more than 5° with changes in bite point. As with lateral and medial gage sites, ventral strain orientations in the FEM vary less with changes in bite point on the balancing side (Fig. 3) than on the working side (Figs 2 and 4). Unlike the lateral and medial aspects of the mandible, strain orientations are more variable between ventral gage sites during middle biting than during posterior biting (Fig. 4). This may be due to the more anterior location of ventral gages (thus, orientations reflect the proximity of bite point). Alternatively, high variability in

Table 10 Circular statistics for bone strains from the ventral aspect of the *Alligator* mandible.

Experiment and Site	56 Ant. ventral dentary		56 Post. ventral dentary		56 Angular		75 Ventral dentary		99 Ventral dentary		102 Ventral dentary		102 Ventral splenial		103 Ventral dentary	
Side	WS	BS	WS	BS	WS	BS	WS	BS	WS	BS	WS	BS	WS	BS	WS	BS
No. of observations	13	10	13	10	13	10	28	45	20	10	47	35	23	22	24	30
Mean vector (μ)	152.212°	3.288°	153.434°	14.397°	68.367°	98.823°	148.328°	61.583°	167.231°	90.704°	137.439°	114.282°	107.664°	86.915°	10.716°	102.267°
Length of mean vector (r)	0.941	0.99	0.966	0.855	0.96	0.649	0.928	1	0.731	0.998	0.682	0.994	0.445	0.906	0.573	0.987
Median	154.4°	2.685°	150.87°	10.72°	66.91°	89.9°	152.915°	61.51°	177.675°	90.2°	141.32°	115.73°	103.02°	87.35°	21.105°	103.31°
Concentration	6.896	34.623	11.556	2.719	9.983	1.614	7.234	1273.631	2.215	221.44	1.901	77.888	0.994	5.61	1.402	39.842
Circular variance	0.029	0.005	0.017	0.072	0.02	0.175	0.036	1.96E-04	0.134	8.16E-04	0.159	0.003	0.277	0.047	0.214	0.006
Circular Standard deviation	9.948°	4.158°	7.585°	16.018°	8.185°	26.615°	11.066°	0.803°	22.676°	1.637°	25.057°	3.257°	36.437°	12.726°	30.247°	4.568°
Standard error of mean	3.118°	1.548°	2.379°	5.941°	2.567°	8.848°	2.089°	0.12°	5.034°	0.609°	3.67°	0.55°	8.98°	2.709°	6.525°	0.834°
95% Confidence interval	146.098°	0.254°	148.77°	2.751°	63.336°	81.477°	144.232°	61.348°	157.363°	89.51°	130.245°	113.203°	90.06°	81.604°	357.924°	100.632°
(−/+) for μ	158.325°	6.323°	158.097°	26.043°	73.399°	116.169°	152.424°	61.818°	177.1°	91.898°	144.632°	115.361°	125.267°	92.226°	23.508°	103.901°
99% Confidence interval	144.178°	359.301°	147.306°	359.093°	61.755°	76.028°	142.945°	61.275°	154.263°	89.134°	127.985°	112.864°	84.531°	79.936°	353.906°	100.118°
(−/+) for μ	160.245°	7.276°	159.561°	29.701°	74.98°	121.618°	153.711°	61.891°	180.2°	92.274°	146.892°	115.7°	130.797°	93.895°	27.526°	104.415°
Rayleigh test (Z)	11.523	9.792	12.12	7.315	11.981	4.218	24.119	44.965	10.689	9.967	21.87	34.551	4.562	18.06	7.872	29.247
Rayleigh test (P)	1.14E-06	< 1E-12	1.33E-06	8.58E-05	1.30E-06	0.011	1.79E-10	< 1E-12	4.15E-06	< 1E-12	2.46E-10	< 1E-12	0.009	2.39E-08	2.10E-04	2.56E-12
Watson's U² test (U²)	0.138	0.056	0.23	0.336	0.138	0.167	0.196	0.137	0.223	0.284	0.186	0.381	0.374	0.978	0.29	0.51
Watson's U² test (P)	< 0.025	0.5 > P > 0.25	< 0.005	< 0.005	< 0.025	< 0.005	< 0.005	< 0.05	< 0.005	< 0.005	< 0.005	< 0.005	< 0.005	< 0.005	< 0.005	< 0.005
Test for WS/BS differences																
W	18.294		18.294		14.356		54.593		20.593		54.495		32.683		43.03	
P	1.07E-04		1.07E-04		7.63E-04		1.40E-12		3.38E-05		1.47E-12		8.00E-08		4.53E-10	
Circular-linear correlation																
r	0.850	0.977	0.864	0.675	0.770	0.747	0.575	0.740	0.619	0.795	0.669	0.735	0.755	0.943	0.838	0.712
P	0.196	0.018	0.088	0.419	0.308	0.344	0.443	0.292	0.155	0.848	0.056	0.027	0.267	0.341	0.168	0.161

*Indicates a result could not be calculated.

Table 11 Two-way ANOVA comparing variation within individual gage sites or between research subjects ('Individual') and with changes in bite location ('Bite Point') in four regions of the *Alligator mandible.*

Dorsolateral WS				Dorsolateral BS			
Source	df	CHI2	*P*-value	Source	df	*F*	*P*-value
'Individual'	4	7.96897	0.092721	'Individual'	2	17.46796	0.003149
'Bite Point'	6	41.2755	2.56E-07	'Bite Point'	3	3.814009	0.076628

Lateral WS				Lateral BS			
Source	df	CHI2	*P*-value	Source	df	CHI2	*P*-value
'Individual'	6	211.6827	0	'Individual'	6	244.7956	0
'Bite Point'	8	16.09427	0.04105	'Bite Point'	8	16.38079	0.037243

Medial WS				Medial BS			
Source	'df'	'CHI2'	'*P*-value'	Source	'df'	'CHI2'	'*P*-value'
'Individual'	6	54.52522	5.78E-10	'Individual'	6	213.2399	0
'Bite Point'	8	71.97532	1.98E-12	'Bite Point'	8	7.993922	0.434064

Ventral WS				Ventral BS			
'Source'	'df'	'CHI2'	'*P*-value'	'Source'	'df'	'CHI2'	'*P*-value'
'Individual'	14	168.7355	0	'Individual'	14	303.9026	0
'Bite Point'	8	48.30766	8.63E-08	'Bite Point'	8	33.75298	4.50E-05

strain orientations on the ventral aspect of the FEM may be a result of numerous sutural contacts – note that during middle biting, there is a distinct line of reversal in strain orientation between the splenial and dentary bones.

Because of high variability in *in vivo* principal strain orientations on the ventral surface of the mandible during ipsilateral biting, strain orientations in the working side FEM broadly overlap *in vivo* strain orientations at all gage sites except the posterior dentary gage of Experiment 56. The range of strain orientations predicted by the balancing side FEM resembled *in vivo* ε_1 orientations recorded in Experiments 75, 99 and 103 during contralateral biting but did not match strain orientations from Experiments 56 or 102.

Principal strain magnitudes and ratios

Within-gage *in vivo* ε_1 means (Tables 2–6) ranged from 34 to 1679 $\mu\varepsilon$ and the grand mean for all gage sites was 924 $\mu\varepsilon$. Within-gage *in vivo* ε_2 means ranged from -145 to -1849 $\mu\varepsilon$ with a grand mean of -955 $\mu\varepsilon$ for all gage sites. There was no difference in mean ε_1 strain magnitudes on the working and balancing sides (Table 12); in contrast, mean ε_2 strain magnitudes were greater on the balancing side. During both ipsilateral and contralateral biting, *in vivo* principal strain magnitudes were higher in the dentary than in the splenial.

The grand $\varepsilon_1/\varepsilon_2$ mean for all *in vivo* experiments was 1.18. The $\varepsilon_1/\varepsilon_2$ ratio was usually > 1 on the working side mandible as a whole as well as in the working side dentary, but < 1 on the balancing side mandible and dentary. These results indicate that the working side mandible (all bones) and the dentary experience predominantly tension, whereas these structures on the balancing side experience predominantly compression. The $\varepsilon_1/\varepsilon_2$ ratio was < 1 in the splenial during both ipsilateral and contralateral biting, suggesting that the splenial is primarily under compression.

ε_1 and ε_2 strains were between two and five times higher during *in vivo* experiments than those exhibited by the FEM (Table 12). Like the *in vivo* results, the FEM exhibited higher ε_2 strains (as well as higher ε_1 strains) on the balancing side than on the working side. Unlike the *in vivo* results, strains were not consistently higher in the dentary of the FEM than in the splenial. $\varepsilon_1/\varepsilon_2$ ratios in the FEM were always higher on the working side than on the balancing side. Unlike the *in vivo* experiments, in which the splenial was always in compression, only the balancing side splenial of the FEM exhibited an $\varepsilon_1/\varepsilon_2$ ratio < 1.

Shear strain

Within-gage means of *in vivo* maximum shear strain ranged from 197 to 3528 $\mu\varepsilon$, the grand mean for all gage sites being

Table 12 Mean shear and principal strain magnitudes across all bite points for different region of the mandible, *in vivo* and *in silico*. Bold values indicate significant results.

	In vivo experiments				FEM		
	Shear strain				Shear strain		
	Grand mean	WS mean	BS mean	*P*-value	Grand mean	WS mean	BS mean
All gage sites	1879	1630	< 2130	**<0.001**	518	339	< 696
Dentary	2122	1809	< 2449	**<0.001**	504	346	< 661
Splenial	1373	1240	< 1498	**0.03**	545	312	< 778
	E1				E1		
	Grand mean	WS mean	BS mean	*P*-value	Grand mean	WS mean	BS mean
All gage sites	924	920	= 928	0.85	208	157	< 258
Dentary	1110	1083	= 1138	0.34	224	161	< 286
Splenial	536	562	= 512	0.3	202	170	< 233
	E2*				E2*		
	Grand mean	WS mean	BS mean	*P*-value	Grand mean	WS mean	BS mean
All gage sites	−955	−710	< −1201	**<0.001**	−310	−182	< −438
Dentary	−1012	−725	< −1310	**<0.001**	−280	−185	< −375
Splenial	−837	−678	< −986	**<0.001**	−343	−141	< −545
	E1/E2				E1/E2		
	Grand mean	WS mean	BS mean	*P*-value	Grand mean	WS mean	BS mean
All gage sites	1.18	1.6	> 0.84	**<0.001**	1.95	2.98	> 0.92
Dentary	1.4	1.88	> 0.95	**<0.001**	2.07	2.95	> 1.19
Splenial	0.77	0.94	> 0.61	**<0.001**	2.1	3.71	> 0.5

*More negative E2 considered to be greater (higher compressive strain).

1879 $\mu\varepsilon$ (Table 12). When all gage sites were considered, there was a significant difference between mean shear strain on the working side and balancing side (1630 vs. 2130 $\mu\varepsilon$, respectively, $P < 0.001$). Similarly, when examined by region of the mandible, mean shear strain was greater on the balancing side than on the working side in both the dentary and splenial bones (Table 12). On both sides, shear strain was higher in the dentary than in the splenial. Shear strain was also higher on the balancing side in the FEM but shear was not higher in the dentary of the FEM than in the splenial. As with principal strain magnitudes, *in vivo* shear strains were between two and four times higher than those exhibited by the FEM.

Strain gradients

Figures 5 and 6 compare mean ε_1 and shear strain magnitudes at every gage site *in vivo* and in the FEM. Strain magnitudes vary greatly among *in vivo* gage sites. Gages on the ventral aspect of the mandible recorded both the highest

(Experiment 75) and lowest (Experiment 56) strains. Higher strains were recorded on the lateral aspect than on the medial aspect of the mandible during both ipsilateral and contralateral biting. Posterior bites generated the highest ε_1 strains at most (but not all) gage sites in the working side mandible; in contrast, middle bites tended to produce both the highest ε_1 and shear strains in the balancing side mandible.

Absolute strain magnitudes are substantially lower in the FEM than *in vivo* at nearly all sites (Figs 5 and 6). As with *in vivo* strains, the ventral aspect of the mandible featured the lowest strains (gage sites corresponding to Experiment 56) and one of the highest strains (gage site corresponding to Experiment 75); in contrast, strains on the lateral aspect of the FEM were not consistently higher than those on the medial aspect. On the working side, posterior bites usually produced the highest strains; there was little variation in strain magnitude with changes in bite location on the balancing side of the FEM.

Table 13 ANOVA testing for differences in ε_1 principal strain orientation during biting at different locations along the toothrow.

Gauge location	Experiment number	Working side bite points represented*	P-value for working side differences**	Balancing side bite points represented*	P-value for balancing side differences**
Dorsolateral dentary	99	2–5	n.s.	3, 5	0.008
	102	2–5	<0.0001	3–5	0.007
	103	2–5	0.003	2–5	n.s.
Lateral dentary	75	2–5	n.s.	1–5	0.003
	99	2–5	n.s.	1, 3–5	n.s.
	102	1–5	n.s.	1–5	<0.0001
	103	2–5	n.s.	2–5	0.007
Ventral dentary	56	2–5	0.016	1, 5	0.007
	56	2–5	0.007	1,5	n.s.
	75	2–5	<0.0001	1–5	<0.0001
	99	2–5	<0.0001	1, 3–5	n.s.
	102	1–5	<0.0001	1–5	n.s.
	103	2–5	<0.0001	2–5	n.s.
Ventral angular	56	2–5	n.s.	1,5	n.s.
Ventral splenial	102	1–5	<0.0001	1–5	n.s.
Medial splenial	75	2–5	0.006	1–5	n.s.
	99	2–5	<0.0001	1, 3–5	0.047
	102	1–5	<0.0001	1–5	n.s.
	103	2–5	<0.0001	2–5	n.s.

*Bite points 1–5 represent bite regions from anterior to posterior.
**P-values represent existence of significant differences among all ε_1 principal strain orientations at bite points represented.

Contour plots of von Mises strain in the FEM reveal strain gradients throughout the mandible during biting (Fig. 7). On both sides of the lower jaw, the articulars, surangulars, ventral angulars, and bone around the external mandibular fenestrae exhibit high strains. Additionally, the ventral aspect of the balancing side ramus (dentary and splenial) experiences high strains. The working side ramus is less strained overall than the balancing side but exhibits high strain immediately below the bite point.

In vivo neutral axis

Neutral axis orientation in the working and balancing sides is presented for different bite points and experiments (Figs 8 and 9, Table 14). The orientation of the neutral axis is measured relative to the horizontal, with positive and negative angles indicating clockwise and counterclockwise rotations, respectively. Note that while the neutral axis orientation is a calculated value based on strain at individual gages, its location relative to the cortex was arbitrarily placed through the center of the cross-section.

On the working side, neutral axis orientations exhibit increased variability as bite point moves from anterior to posterior; the range of neutral axis orientations across all experiments is 68.9, 98.0, 118.3 and 104.6° for anterior/middle, middle, middle/posterior and posterior bite points, respectively. Although mean neutral axis orientations across bite points and experiments show some degree of consistency, they provide conflicting results in terms of bending regime. In two experiments (102 and 103), mean neutral axis orientations indicate negative dorsoventral bending (i.e. the dorsal border of the mandible under tension). However, in Experiment 75 the dorsal border is under compression. Finally, in Experiment 99 the mean neutral axis orientation indicates mediolateral bending. Maximum and minimum normal strains on the working side are similarly variable (Fig. 8, Table 14). Absolute normal strains range from 5780 $\mu\varepsilon$ (anterior/middle biting, Experiment 103) to -6130 $\mu\varepsilon$ (posterior biting, Experiment 75). In two experiments (Experiment 75 and 102), maximum and minimum normal strains increase with more posterior bites, but no obvious trend exists in Experiments 99 and 103. In summary, neutral axis orientations for the working side are variable, with little consistency across experiments and large standard deviations within experiments.

In contrast, average neutral axis orientations on the balancing side show little variation, either across different bite point locations or across experiments (Fig. 9, Table 14). The exception is Experiment 99, which exhibits high variability, both within and across bite points. For Experiments 75, 102, and 103, mean neutral axis orientation for all contralateral bite point locations ranges from 1.8 to 26.8°. This suggests that the balancing side consistently experiences negative dorsoventral bending (the dorsal border under tension). Additionally, there may be some lateral bending (with the lateral aspect of the mandible under tension), as indicated by the consistent counterclockwise rotation of the neutral axis. Maximum normal strains on the balancing side are similar to those on the working side but minimum normal strains are not as extreme as those recorded on the

Working side   Balancing side

Lateral
Middle

Posterior

Medial
Middle

Posterior

Ventral
Middle

Posterior
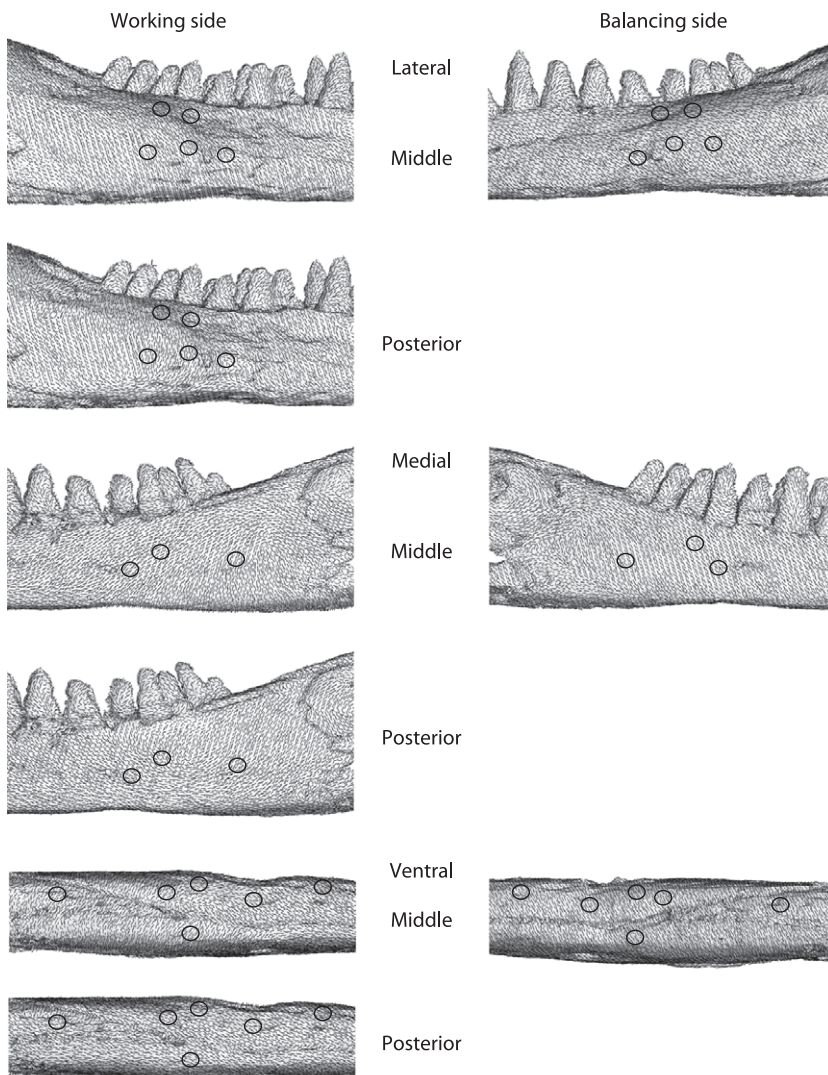
Fig. 4 Strain fields in the FEM (finite element model). Vectors indicate maximum principal strain orientations at the centroid of each element in the FEM in lateral (top) medial (middle) and ventral (bottom) views of the working and balancing sides of the model. Note that the working side in the FEM is the right mandible and the balancing side is the left mandible. Black circles indicate the location of *in vivo* gage sites from which data was extracted. Strain fields generated in the working side during middle and posterior bites are shown to illustrate the impact of bite point on strain orientations; strain fields showed little variability with change in bite point on the balancing side, thus only middle bites are illustrated.

working side. There is no clear trend of increasing or decreasing normal strains for different bite points. In summary, neutral axis orientations on the balancing side, with the exception of one experiment, show low variability across contralateral bite points or experiments.

FEM neutral axis

Strain normal to the middle posterior section of the *Alligator* FEM during biting at different locations is illustrated for the working (Fig. 8) and balancing (Fig. 9) sides, and neutral axis orientation and strain magnitudes are listed in Table 14. Unlike the *in vivo* neutral axis, which is assumed to be straight, the FEM indicates that the neutral axis is more sinuous and its course is influenced by internal structures such as sutures, cavities and tooth roots. Nonetheless, the neutral axis in the FEM passes near the section geometric centroid in nearly all cases.

On the working side, the neutral axis of the *Alligator* FEM rotates counterclockwise as bite point moves from anterior/middle to posterior (Fig. 8). During anterior biting, the dorsal margin of the mandible is under tension, whereas the ventral border experiences compression, indicating negative bending. During middle bites, compressive strain shifts to the lateral aspect of the mandible and tension occurs on the medial aspect, suggesting the mandible is being bent medially. During middle posterior and posterior bites, the neutral axis is obliquely oriented, with compression occurring dorsally and laterally, and tension located ventrally and medially, indicating positive bending of the mandible with some medial bending.

On the balancing side, the orientation of the neutral axis does not change with changes in contralateral bite point, being obliquely oriented through the corpus. The dorsal margin of the mandible is always in tension, whereas its ventral border is in compression, indicating negative bending. Because compression is shifted slightly to the medial surface (and tension is shifted laterally), there also appears to be some lateral bending of the balancing side.

© 2013 Anatomical Society
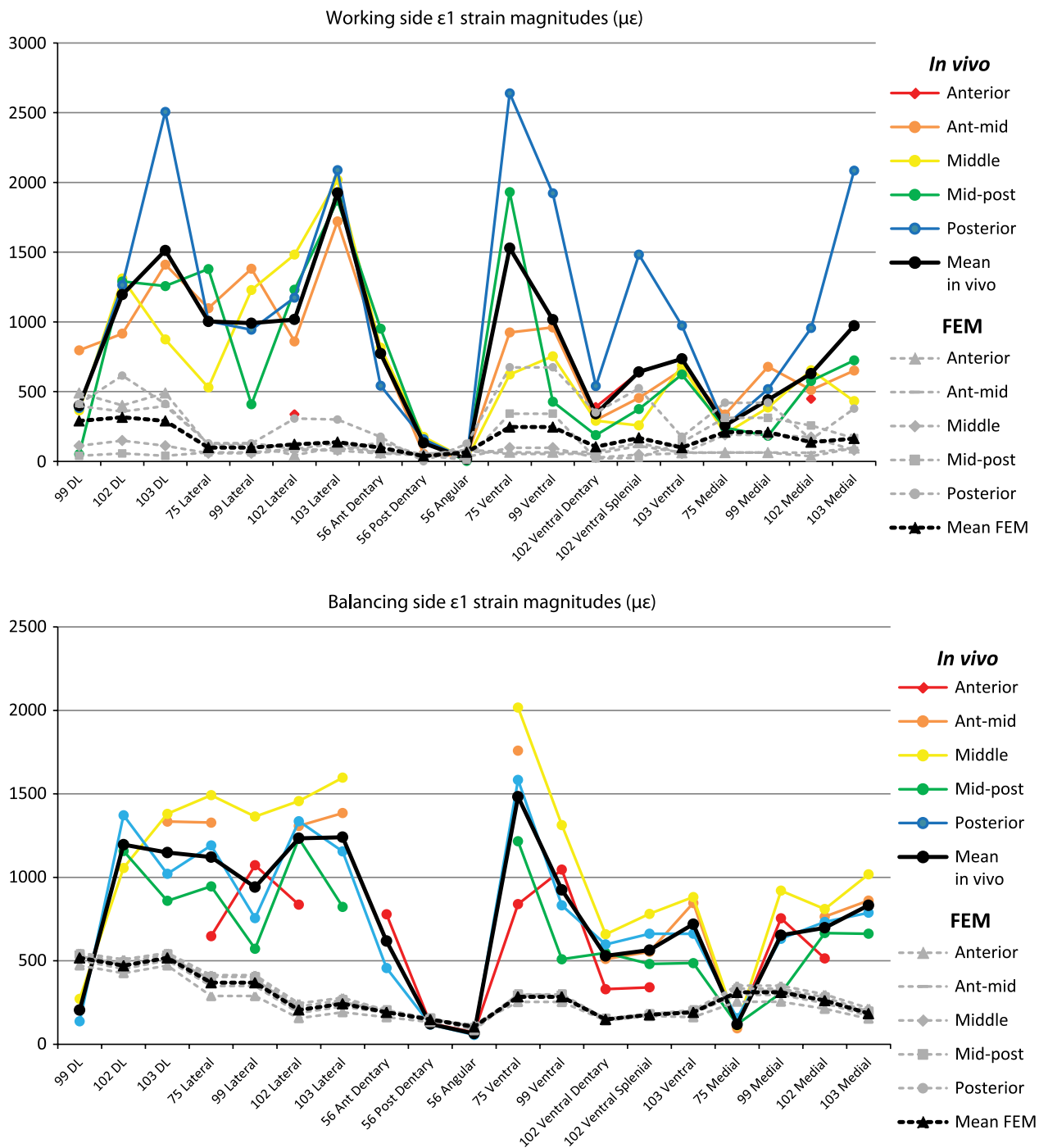
Fig. 5 Mean *in vivo* and FEM (finite element model) ε_1 strain magnitudes. Plots illustrate maximum principal strain at 19 gage sites and their corresponding sites in the FEM. The upper plot shows results from the working side and the lower plot shows results from the balancing side. Both the mean ε_1 strains within each gage site and the mean value during biting at different locations are shown. Missing areas of the *in vivo* plots indicate no data was collected for this bite point at this gage site.

Because of the variability in the orientation of the working side neutral axis observed *in vivo*, it is difficult to compare neutral axis orientations between the *Alligator* FEM and *in vivo* results. In contrast, neutral axis orientations are very similar on the balancing side of the *in vivo* experiments (except Experiment 99) and the FEM.

Maximum and minimum normal strain magnitudes are lower in the FEM than those calculated *in vivo*. On the working side, strain magnitudes vary with changes in bite point; on the balancing side, magnitudes are consistent despite changes in bite location.
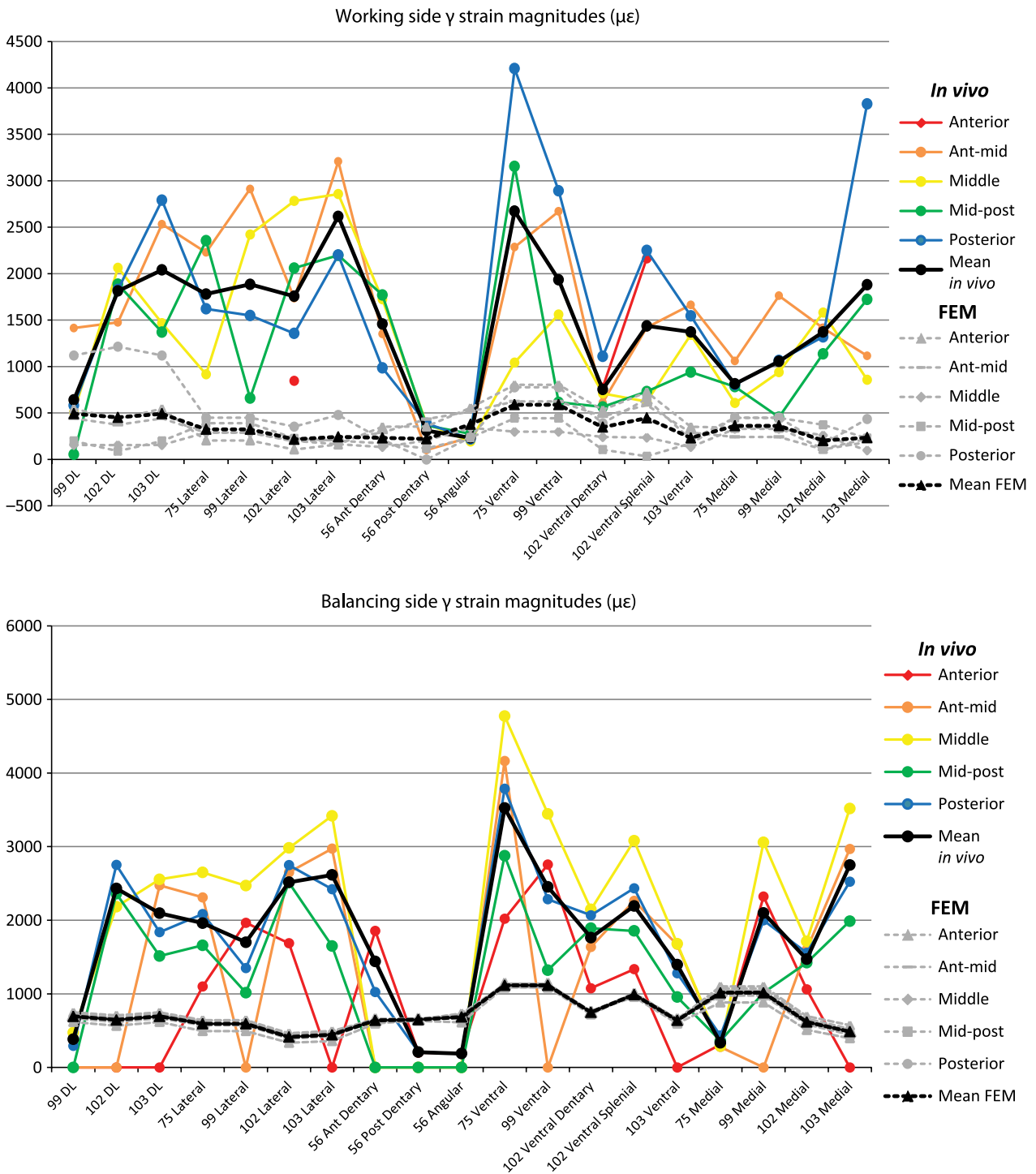
Fig. 6 Plots comparing mean *in vivo* and FEM (finite element model) shear (γ) strain magnitudes. Plots illustrate shear strain at 19 gage sites and their corresponding sites in the FEM. The upper plot shows results from the working side and the lower plot from the balancing side. Both the mean γ strains within each gage site and the mean value during biting at different locations are shown.

Discussion

We have presented new *in vivo* bone strain data from the *Alligator* mandible, including strain orientations and magnitudes, and neutral axis of bending; the same data were extracted from the FEM. Here we evaluate our FEM using *in vivo* data, then use the FEM to understand overall deformation and strain distribution in the mandible during biting. Finally, we compare *Alligator* strain data and deformation regimes with those known from mammalian mandibles.
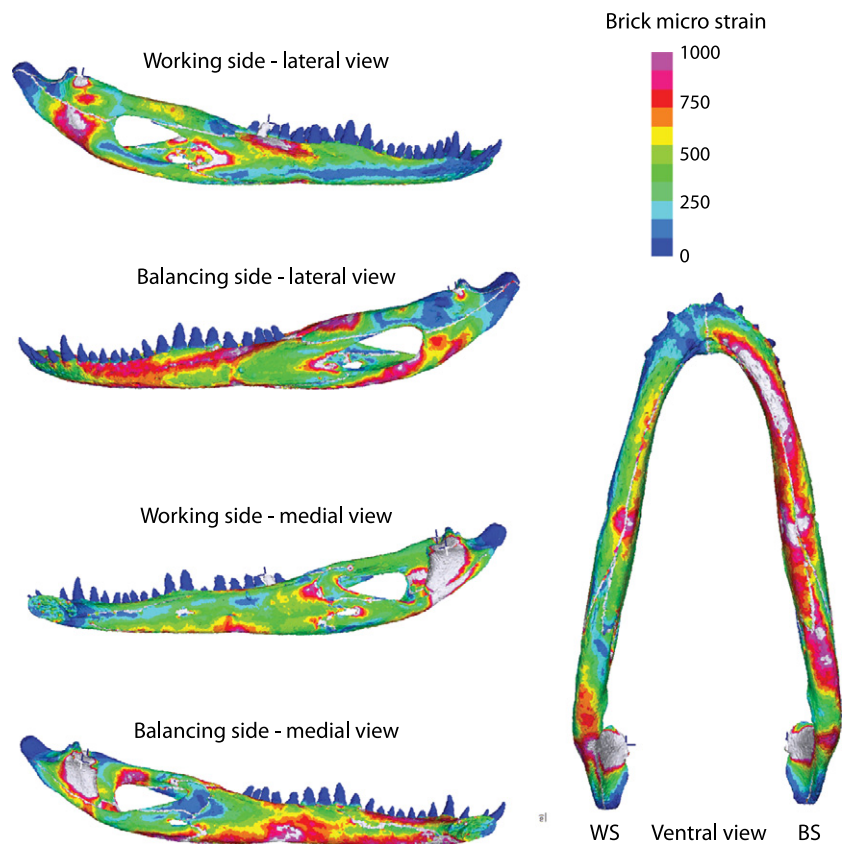
Fig. 7 Contour plots of von Mises strain in the FEM (finite element model). Scale bar indicates strain magnitude (in microstrain) during posterior biting. WS, working side; BS, balancing side in ventral view. For the FEM, the right mandible is always the working side, the left mandible is the balancing side.

Some problems with the data should be noted. First, due to animal behavior and gage failure, complete datasets are not available for all experiments. Secondly, some experiments gave results that were inconsistent with other experiments; most notable are the results for orientation of the neutral axis in Experiment 99 (Figs 8 and 9) and the principal strain orientations from the lateral gage in Experiment 103 (Figs 2 and 3).

FEM validation and mandibular deformation

Overall, there is a good correspondence between *in vivo* and *in silico* principal strain orientations, including changes in strain orientations with changes in bite point. FEM ε_1 strain orientations overlap orientations recorded *in vivo* at 17 of 19 gage sites during ipsilateral biting and at 10 of 19 sites during contralateral biting. The greatest discrepancy between *in vivo* and FEM strain orientations occurred on the ventral aspect of the mandible during contralateral biting, during which FEM ε_1 strain orientations overlapped *in vivo* orientations at only three of eight gage sites. It should be noted that strain orientations at three ventral gage sites in Experiment 56, which did not match those obtained from the FEM, also showed poor correspondence with ventral strain orientations obtained in other experiments (Fig. 3). Additionally, strain fields from the ventral aspect of the FEM demonstrate that strain orientations are highly vari-

able between gage sites. Thus, although our FEM does not perfectly represent mandibular deformation during biting, general agreement between *in vivo* and *in silico* surface strain orientations and the location/orientation of the neutral axis of bending through the corpus suggest our FEM is a reasonable working hypothesis of mandibular deformation in *Alligator* during biting. The poor correspondence between *in vivo* and FEM surface strains along the ventral aspect of the mandible may be due these areas being adjacent to sutures, the modeling of which may be imprecise (Reed et al. 2011).

In vivo principal strain orientations and the FEM are used to describe deformation in the mandible during biting. As noted in previous studies (Chalk et al. 2011; Porro et al. 2011; Ross et al. 2011), the FEM itself (its geometry, material properties, and boundary conditions) is our hypothesis of the mechanical behavior of the *Alligator* mandible; the following descriptors simply summarize the deformation undergone by the mandible during biting.

Analysis of the working side FEM (Fig. 8, and see Porro et al. 2011) suggests that the middle-posterior section of the mandible (where most gages were placed) experiences negative bending (dorsal deformation) during anterior bites, but positive bending (ventral deformation) as the bite point moves posteriorly. Dynamic deformation videos of the FEM (Supporting Information Video S1) illustrate how, during anterior bites, the upward action of the jaw elevator
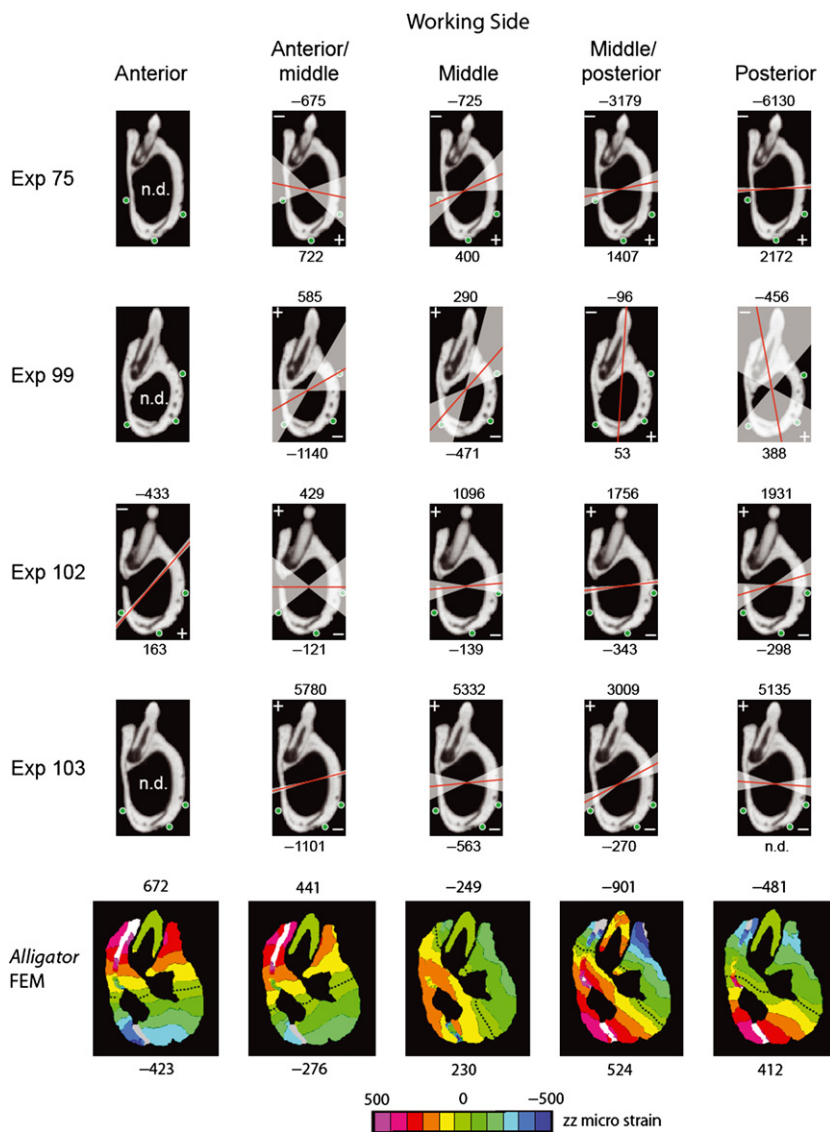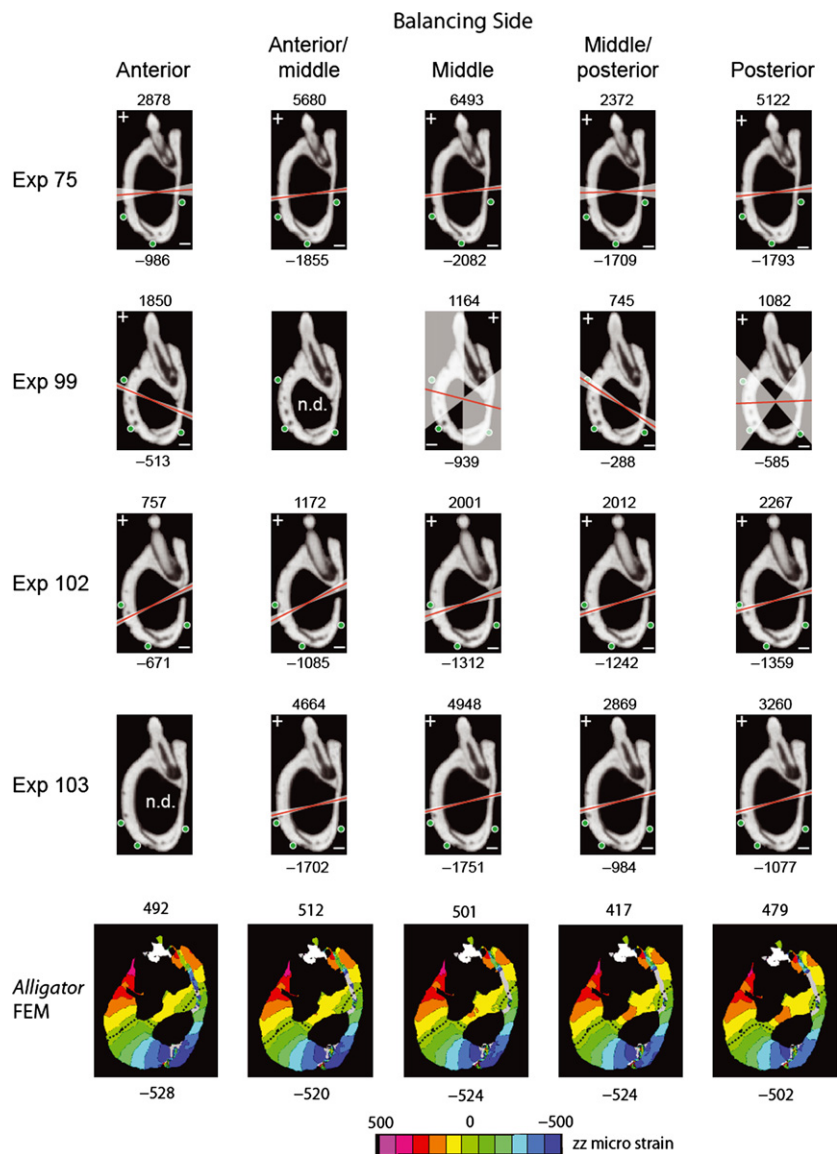
Fig. 8 Orientation of the neutral axis through the working side. Neutral axis is shown within corpus cross-sections from *in vivo* experiments and the FEM during biting at five points. All images represent a section of the right mandible (middle-posterior region) viewed from the rear. For all sections, maximum and minimum normal strains in these sections are shown above and below the section. *In vivo* sections are CT scans taken from individual research subjects at the section of the gages. For *in vivo* sections, the red line indicates the neutral axis (assumed to be straight and to pass through the section centroid); the gray areas on either side of the neutral axis indicate one standard deviation. Green circles indicate the location of the gages in each experiment. N.d., no data for a bite point. For the FEM sections, colors indicate the magnitude and type of normal strain (tension as positive values and 'hot' colors, compression as negative values and 'cool' colors). The neutral axis passes through the center of the light green contour and is shown as a black dotted line. Very high tensile strains (especially in sutures) are shown in white and very high compressive strains in gray.

muscles results in the mandible being bent dorsally. During posterior bites, the posterior portion of the mandible experiences dorsal deformation, whereas the portion anterior to the bite point experiences ventral deformation due to forces. At all bite points, the working side mandible is deformed medially, and the ventral margin of the mandible is inverted while the tooth row is everted, indicative of torsion (*sensu* Figs 9 and 14 in Porro et al. 2011). As in the FEM, during anterior biting in most *in vivo* experiments ε_1 is directed anteroinferiorly on the upper lateral aspect of the working side, rotating clockwise as bite point shifts posteriorly. Strains on the ventral surface of the mandible were directed along the long-axis of the mandible and rotated counterclockwise with a posterior shift in bite point. These strain orientations suggest a combination of negative dorsoventral bending and positive torsion of the working side mandible (eversion of anterior toothrow relative to gaged sections) during anterior biting. As the

bite point moves posteriorly, positive bending becomes more important.

Examination of the balancing side FEM (Fig. 9, and see Porro et al. 2011) reveals that, regardless of bite point on the working side mandible, the most important deformation regime on the balancing side is (negative) dorsoventral bending, i.e. the mandible is bent upwards in the middle so that the dorsal edge is in longitudinal tension and the ventral edge is in longitudinal compression. This loading regime is due to the upwardly directed action of the jaw elevators being opposed at the symphysis and jaw joint. The second most important deformation regime in the balancing side mandible is torsion due to inversion of the anterior toothrow relative to the section of the mandible where strain was recorded. Dynamic views of the FEM show inversion of the balancing side tooth row (Supporting Information Videos S1 and S2). *In vivo*, the lateral orientation of ε_1 on the ventral surface of the balancing side mandible is

Fig. 9 Orientation of the neutral axis through the balancing side. Neutral axis is shown within corpus cross-sections from *in vivo* experiments and the FEM during biting at five contralateral points. All images represent a section of the right mandible (middle-posterior region) viewed from the rear. For all sections, maximum and minimum normal strains in these sections are shown above and below the section. *In vivo* sections are CT scans taken from individual research subjects at the section of the gages. For *in vivo* sections, the red line indicates the neutral axis (assumed to be straight and pass through the section centroid); the gray areas on either side of the neutral axis indicate one standard deviation. Green circles indicate the location of the gages in each experiment. N.d., no data for a bite point. For the FEM sections, colors indicate the magnitude and type of normal strains (tension as positive values and 'hot' colors, compression as negative values and 'cool' colors). The neutral axis passes through the center of the light green contour and is shown as a dotted line. Very high tensile strains are shown in white and very high compressive strains in gray.

indicative of negative dorsoventral bending regime. Moreover, the anterosuperiorly directed components of ε_1 on the lateral aspect of the mandible *in vivo* and the anteroinferiorly directed components on the medial aspect are suggestive of the torsional regime described above. As in the FEM, *in vivo* balancing side strain orientations change little with changes in bite location. Cross-sections through both the *in vivo* mandible and FEM (Fig. 9) corroborate predictions from strain orientations, demonstrating that the mandible is being bent dorsally (negative bending) at all bite points, although slight counterclockwise rotation of the neutral axis suggests some lateral bending.

For all gage sites in all experiments, ε_1 orientation during ipsilateral biting is both different from and more variable (with changes in bite point) than during contralateral bites – 13 of the 19 gages exhibited statistically significant differences in ε_1 orientations ($P < 0.05$) for different bite points

during ipsilateral bites; only eight of 19 gage sites exhibited significant differences in ε_1 orientations with changes in bite point during contralateral bites (Table 13). The orientation of the neutral axis is also more variable on the working side than on the balancing side. Thus, both *in vivo* and *in silico* results clearly demonstrate the impact of bite force and bite location on the mechanical behavior of the working side. Furthermore, inter-experimental variation in ε_1 orientation is greater on the working side than on the balancing side. Lastly, on the working side, variation in ε_1 orientation is lowest on the lateral aspect of the mandible (mean $r = 0.83$), and highest on the medial aspect (mean $r = 0.49$); whereas on the balancing side, variation in ε_1 orientation was lowest on the medial aspect of the mandible (mean $r = 0.97$).

Circular-linear analyses reveal correlations between strain orientation and magnitude at some gage sites. These correlations are not unexpected as there can only be one load-

Table 14 Descriptive statistics for orientation of neutral axis of bending (α) and calculated maximum and minimum normal strains for all experiments and the FEM.

Experiment	Bite side	Bite position*	n	Neutral axis orientation (α)		Maximum calculated normal strain (με)		Minimum calculated normal strain (με)	
				Mean	SD	Mean	SD	Mean	SD
75	Left (WS)	a/m	4	11.6	32.4	722	580	−675	381
		m	6	−24.1	23	400	246	−725	822
		m/p	12	−11.8	15.1	1407	888	−3179	2729
		p	8	−2.8	2.7	2172	844	−6130	2463
	All left		**30**	**−8.8**	**20.2**	**1318**	**972**	**−3142**	**2989**
	Right (BS)	a	4	4.3	8.5	2878	659	−986	198
		a/m	3	7.4	0.9	5680	931	−1855	271
		m	19	6.5	1.2	6493	1518	−2082	470
		m/p	8	1.8	9.7	2373	2018	−1709	1414
		p	5	6.2	4.6	5122	2375	−1793	670
	All right		**39**	**5.5**	**5.3**	**5056**	**2367**	**−1829**	**774**
	All bites		**69**	**0.1**	**14.8**	**3637**	**2671**	**−2328**	**2025**
99	Right (WS)	a/m	2	30	30.3	585	186	−1140	676
		m	9	48.8	26.1	290	188	−471	312
		m/p	1	86.3		53		−96	
		p	9	100.5	50.9	388	193	−456	475
	All right		**21**	**69.6**	**46**	**346**	**206**	**−508**	**444**
	Left (BS)	a	2	22.6	1.7	1850	431	−513	126
		m	3	−37.6	52.3	1164	337	−939	535
		m/p	7	33.5	3.4	745	310	−288	71
		p	3	−2.4	51.5	1082	725	−575	219
	All left		**15**	**10.6**	**39.9**	**1044**	**535**	**−506**	**340**
	All bites		**36**	**45.9**	**52.1**	**629**	**507**	**−507**	**400**
102	Left (WS)	a	2	−49.1	1.8	163	8	−433	149
		a/m	9	0.1	38.3	429	402	−121	183
		m	19	−5	14.4	1096	561	−139	167
		m/p	6	−6.9	4.3	1756	1232	−343	319
		p	9	−16.6	19.1	1931	803	−298	384
	All left		**45**	**−8.5**	**23**	**189**	**880**	**−212**	**258**
	Right (BS)	a	2	26.5	2.4	757	36	−671	46
		a/m	2	26.8	4.7	1172	439	−1055	281
		m	9	18.1	6.9	2001	695	−1312	440
		m/p	11	17.1	2.6	2012	927	−1242	547
		p	12	15.3	3.4	2267	1146	−1359	654
	All right		**36**	**17.8**	**5.4**	**1978**	**962**	**−1256**	**541**
	All bites		**81**	**3.2**	**22**	**1532**	**986**	**−674**	**653**
103	Right (WS)	a/m	9	14.5	3	5780	1010	−1101	436
		m	3	5.6	19.7	5332	2985	−563	47
		m/p	4	28.3	11.2	3009	1425	−270	
		p	8	−4.1	14.2	5135	1501		
	All right		**24**	**9.5**	**15.9**	**5047**	**1739**	**−645**	**241**
	Left (BS)	a/m	6	13.3	3.1	4664	1063	−1702	355
		m	3	13.6	0.4	4948	945	−1751	282
		m/p	6	12.1	4.4	2869	1295	−984	498
		p	4	14.9	5	3260	1193	−1077	438
	All left		**19**	**13.6**	**3.7**	**3846**	**1392**	**−1351**	**524**
	All bites		**43**	**−43.5**	**45.7**	**3137**	**1486**	**−2191**	**1447**

Table 14. (continued)

Experiment	Bite side	Bite position*	n	Neutral axis orientation (α)		Maximum calculated normal strain (με)		Minimum calculated normal strain (με)	
				Mean	SD	Mean	SD	Mean	SD
FEM	Right (WS)	a		7		672		−423	
		a/m		21		441		−276	
		m		−62		230		−249	
		m/p		−43		524		−901	
		p		−23		412		−381	
	All left			**−20**		**456**		**−446**	
	Left (BS)	a		28		492		−528	
		a/m		31		512		−520	
		m		31		501		−524	
		m/p		31		417		−524	
		p		30		479		−502	
	All right			**30**		**480**		**−520**	
	All bites			**5**		**468**		**−483**	

a, anterior; a/m, anterior/middle; m, middle; m/p, middle/posterior; p. posterior.

ing/stress/strain regime during maximal contraction of the jaw elevator muscles. As muscle recruitment approaches this value, there are likely to be fewer ways of generating bite force.

Strain magnitudes and gradients

Absolute principal and shear strain magnitudes were substantially lower in our FEM than data recorded at nearly all corresponding gage sites *in vivo*. Good correspondence in principal strain orientation with large discrepancies in principal strain magnitude is common in validation studies of vertebrate skulls, being noted when comparing *in vivo* and FEM results in the crania of primates (Ross et al. 2005, 2011; Kupczik et al. 2009) and crocodilians (Metzger et al. 2005). Better correspondence has been found between FEM and *in vitro* strain magnitudes in validation studies of the macaque mandible (Kupczik et al. 2007; Panagiotopoulou et al. 2010, 2011), ostrich mandible (Rayfield, 2011) and pig cranium (Bright & Rayfield, 2011). However, it should be noted that in some of these studies material properties were changed and models made less stiff before comparable strain magnitudes were obtained in *post hoc* analyses.

Various factors may be responsible for the discrepancy in strain magnitudes between the *in vivo* data and the FEM. We used a value of 300 kN m^{-2} for the specific tension of muscle, a value commonly found in the literature (Sinclair & Alexander, 1987); nonetheless, it is possible that *Alligator* jaw muscle contracts with greater force. Recent multi-body dynamics analyses of the diapsid *Sphenodon* have suggested that the specific tension of jaw muscles in this taxon must be significantly higher (890 kN m^{-2}) to generate bite

forces recorded *in vivo* (Curtis et al. 2010); furthermore, FEA of the skulls of multiple crocodilian species using a specific muscle tension of 300 kN m^{-2} resulted in bite forces consistently and significantly lower than those reported *in vivo* (Erickson et al. 2012; Walmsley et al. 2013). Our model incorporated recently reported material properties for *Alligator* mandibular cortical bone (Zapata et al. 2010); however, there are no data on the material properties of reptilian cranial sutures. It is possible that the Young's modulus assigned to the sutures within our model is too elastic, allowing the sutures to act as 'strain sinks' that decrease strain in surrounding bone (Buckland-Wright, 1978; Rafferty et al. 2003). Moreover, our model does not incorporate less stiff trabecular bone in the articular of the *Alligator* mandible, possibly rendering the model too stiff. Lastly, constraints have a tremendous impact on strain magnitudes within FEMs (Marinescu et al. 2005). We constrained the mandible at three nodes aligned mediolaterally across each articular, as well as a single node on the medial aspect of each mandible. This combination of constraints was found to produce the closest correspondence to *in vivo* data in terms of strain orientations. However, it is possible that our model is over-constrained, resulting in low strain magnitudes. Ongoing sensitivity analyses will shed further light on the input parameters impacting model behavior.

Strain gradients as visualized in FEA contour plots reveal very high strains at the articular and surrounding the external mandibular fenestra, suggesting that morphology in these regions may be better optimized for resisting forces exerted by the jaw adductors and joint reaction forces than those related to bite force. Interestingly, the working side mandibular corpus exhibits low

strains (except immediately below the bite point) while the ventral aspect of the balancing side and the symphysis are highly strained. This concurs with *in vivo* and FEM strain data that demonstrate that the balancing side mandible experiences higher principal and shear strains than the working side.

Form–function relationships in the *Alligator mandible*

Our *in vivo* experiments and FE modeling only addressed the mechanical behavior of the mandible during biting; we did not elicit or attempt to model other feeding behaviors such as prey shaking and body rolling. Nevertheless, some comments regarding form–function relationships in the *Alligator* mandible are possible.

Van Drongelen & Dullemeijer's (1982) analysis of mandible morphology in *Caiman* assumed that resistance to bending stress played a significant role in crocodilian mandible design. Although the *in vivo* and FEM results presented here and in Porro et al. (2011) confirm this assumption, they also suggest that other loading regimes are important, such as torsion and mediolateral bending. Moreover, (Porro et al. 2011) demonstrated that mandibular geometry interacts with bone and suture material properties to improve resistance of the mandible to external forces. A complete optimization analysis of *Alligator* mandible form should take these into account.

How does the *Alligator* mandible withstand the high strains recorded *in vivo* and estimated within cross-sections (Figs 8 and 9)? The strains recorded here are the largest reported from any vertebrate mandible: > 4000 με in tension in the biting side ventral dentary in Experiment 75 (Table 3), and < -3400 με in compression from the same gage on the working side. These values exceed those reported from the limb bones of galloping mammals (Biewener & Taylor, 1986), which are generated when the body mass is supported on one limb, whereas the mandibular strains recorded in our experiments were generated by the jaw elevator muscles alone. Moreover, if our calculations of normal strains in mandibular cross-sections are correct, maximum *normal* strains in the mandible exceed 5000 or even 6000 με in tension (Figs 8 and 9). Given that vertebrate bone yields at around 4500–9400 με under static loading (Currey, 1990), and at even lower magnitudes under repetitive loading conditions, it seems unlikely that *Alligator* mandibles experience these strains regularly. Nevertheless, we conjecture that the defensive bites elicited in experimental settings may have resulted in close to the maximum stress and strains experienced by the *Alligator* mandible.

Comparison of mandible deformation in *Alligator* and mammals

The only other vertebrates for which extensive *in vivo* mandibular bone strain data are available are primate and ungulate mammals. The alligator feeding system differs from that of mammals both structurally (previously discussed) and in various functional aspects, including lack of translation at the craniomandibular joint, the magnitude of the bite forces experienced by the mandible, and the much lower number of daily loading events. These differences make it difficult to isolate reasons for differences in deformation and strain regimes. Nevertheless, some interesting observations are possible.

Free body analysis and *in vivo* bone strains suggest that during mastication and biting, the working side mandible of primates is twisted about its long axis, with the tooth row and mandibular angle being everted. Additionally, the corpus is sheared perpendicular to its long axis and bent in sagittal planes; however, these shear and bending stresses are less important than torsion on the working side. The balancing side primate mandible is bent during mastication, but both bent and twisted during isometric biting (Hylander, 1977, 1979a,b, 1981, 1984).

In *Alligator*, the deformation regime of the balancing side mandible closely resembles that of anthropoid primates, i.e. strong negative bending. In contrast, torsion is much less important than dorsoventral bending in the working side *Alligator* mandible (Porro et al. 2011), a difference attributable to the relatively longer mandible of *Alligator*. The most significant differences between primate and alligator mandible deformation regimes are in the region of the jaw muscle attachments. In primates the laterally directed masseter muscle everts the angle of the mandible (Hylander, 1979b). In contrast, the angle of the *Alligator* mandible is inverted; furthermore, the *Alligator* mandible experiences relatively large mediolateral bending stresses due to the orientation of the jaw elevator muscles, which generate large reaction forces at the jaw joint and pterygoid flange (Porro et al. 2011). The significance of this difference in loading regime for mandibular design in mammalian and non-mammalian vertebrates has yet to be evaluated.

Primates (Hylander et al. 1987), rabbits (Weijs & De Jongh, 1977) and hyraxes (Lieberman et al. 2004) experience different loading regimes on the working and balancing side mandibles; pigs are the only mammal studied to date that show similar loading regimes on the working and balancing sides, which may be related to their isognathous chewing and bilateral mastication (Herring & Scapino, 1973; Herring et al. 2001). Although mammals for which electromyographic data are available show differences in the magnitude and timing of activation between working and balancing jaw elevator muscles, crocodilians are thought to use their jaw elevators synchronously and symmetrically (Van Drongelen & Dullemeijer, 1982; Busbey, 1989; Cleuren & De Vree, 1995). This suggests that differences in stress and strain regimes on working and balancing side in *Alligator* are due to differences in reaction forces.

Concluding remarks

The results presented here document for the first time *in vivo* bone strain in a sauropsid mandible during feeding. The deformation regime (inferred from principal strain orientations and neutral axis orientations) and strain magnitudes described here will serve as a baseline with which the mandibles of other sauropsids can be compared. Such future comparative studies, encompassing crocodilians, extinct archosaurs, squamates and turtles, may highlight similarities or differences in the mechanical response of the mandibles due to diet, feeding behavior and musculature, reflected in either convergent or disparate mandibular morphology.

As part of this study, we compared strain magnitudes and orientations (as well as neutral axes of bending) collected *in vivo* to data produced by a high-resolution FEM. Although this model has been the basis of previous studies, the accuracy of its predictions awaited validation against *in vivo* data. The results presented here suggest that our FEM of the *Alligator* mandible accurately predicts principal strain and neutral axis orientations (and, by extension, deformation regime) during biting at different points along the tooth row. Although FEA results should be validated against *in vivo/in vitro* data when feasible, this is not possible for extinct forms. Our results suggest that given accurate geometry, material properties and boundary conditions, FEMs of sauropsid mandibles can be used to model deformation regimes realistically, highlighting the power of FEA in a comparative context.

In contrast, principal and shear strain magnitudes exhibited by the FEM are substantially lower than those recorded *in vivo*. Potential reasons for this discrepancy have previously been discussed; however, until the underlying cause is identified, we would caution researchers about using *absolute* values obtained from skull FEMs – for example, to predict maximum bite forces or skull safety factors. Furthermore, our FEM/*in vivo* comparison suggests that areas immediately adjacent to the application of loads (jaw joint and bite point) and areas immediately adjacent to sutures experience highly variable strain orientations; results from these areas should be thus be interpreted cautiously.

Both *in vivo* experimental data and the FEM highlight differences in the mechanical behavior of the *Alligator* mandible compared with that of primate mandibles. Although the primary deformation regime of the primate mandible, particularly the working side, is torsion about its long axis, the mandible of *Alligator* experiences a greater degree of dorsoventral bending, due to its relatively greater length. Furthermore, the medial placement of the jaw elevator muscles in diapsids (compared with their medial and lateral placement in mammals) reverses the direction of torsion experienced by the posterior portion of the *Alligator* mandible compared with that of primates. Strain magnitudes recorded in the *Alligator* mandible are much larger than those reported in mammals, and higher even than peak principal strains recorded in the crania of the lizards *Uromastyx* and *Tupinambis* (C. F. Ross, A. Herrel, L. B. Porro, K. Murray, S. Evans and M. Fagan, in review; L.B. Porro, C.F. Ross., J. Iriarte-Diaz, J. O'Reilly, S.E. Evans and M.J. Fagan, unpublished data). Strong strain gradients within the mandible, as illustrated by the FEM, suggest that certain regions of the mandible may be more strongly adapted to resist feeding forces (either reaction forces at the jaw joint or bite point or forces exerted by muscles) than other areas.

Both the *in vivo* and FEM data highlight the impact of bite point on the mechanical response of the mandible. Ongoing sensitivity analyses are evaluating the effect of other input variables, including material properties, constraints and muscle force, on model behavior. The availability of *in vivo* data will allow us to determine not only how these input parameters impact behavior, but also which specific combination produce the most accurate results.

Acknowledgements

Author contributions

All authors conceived of and designed the research. K.A.M. and C.F.R. collected *in vivo* data. K.A.M., C.F.R. and L.B.P. processed and interpreted *in vivo* data. L.B.P. built, loaded and interpreted the FEM. J.I.D. and C.F.R. wrote the MATLAB code for extracting FEM data. J.I.D. extracted and processed surface strain data from the FEM. L.B.P., K.A.M. and C.F.R. drafted the manuscript. All authors read and commented on the manuscript.

References

Bell PR, Snively E, Shychoski L (2009) A comparison of the jaw mechanics in hadrosaurid and ceratopsid dinosaurs using finite element analysis. *Anat Rec (Hoboken)* **292**, 1338–1351.

Berens P (2009) CircStat: a MATLAB toolbox for circular statistics. *J Stat Softw* **31**, p. 21. Available at http://www.jstatsoft.org/v31/i10.

Biewener AA, Taylor CR (1986) Bone strain: a determinant of gait and speed? *J Exp Biol* **123**, 383–400.

Bock WJ (1966) An approach to the functional analysis of bill shape. *Auk* **83**, 10–51.

Bock WJ, Kummer B (1968) The avian mandible as a structural girder. *J Biomech* **1**, 89–96.

Bock WJ, Von Wahlert G (1965) Adaptation and the form-function complex. *Evolution* **19**, 269–299.

Bright JA, Rayfield EJ (2011) Sensitivity and ex vivo validation of finite element models of the domestic pig cranium. *J Anat* **219**, 456–471.

Buckland-Wright JC (1978) Bone structure and the patterns of force transmission in the in the cat skull (*Felis cattus*). *J Morphol* **155**, 35–62.

Busbey AB (1989) Form and function of the feedng apparatus of *Alligator mississippiensis*. *J Morphol* **202**, 99–127.

Busbey AB (1995) The structural consequences of skull flattening in crocodilians. In: *Functional Morphology in Vertebrate Paleontology*. (ed. Thomason JJ), pp. 173–192, Cambridge: Cambridge University Press.

Carter DR, Harris WH, Vasu R, et al. (1981) The mechanical and biological response of cortical bone to *in vivo* strain histories. In: *Mechanical Properties of Bone* (AMD vol. 45). (ed. Cowin SC), pp. 81–92, New York: American Society of Mechanical Engineers.

Chalk J, Richmond BG, Ross CF, et al. (2011) A finite element analysis of masticatory stress hypotheses. *Am J Phys Anthropol* **145**, 1–10.

Cleuren J, Aerts P, De Vree F (1995) Bite and joint force analysis in *Caiman crocodilus*. *Belg J Zool* **125**, 79–94.

Currey JD (1990) Physical characteristics affecting the tensile failure properties of compact bone. *J Biomech* **23**, 837–844.

Currey JD (2002) *Bone: Structure and Mechanics*. Princeton: Princeton University Press.

Curtis N, Jones MEH, Lappin AK, et al. (2010) Comparison between *in vivo* and theoretical bite performance: using multi-body modelling to predict muscle and bite forces in a reptile skull. *J Biomech* **43**, 2804–2809.

Daniel WJT, McHenry C (2001) Bite force to skull stress correlation – modelling the skull of *Alligator mississippiensis*. In: *Crocodilian Biology and Evolution*. (eds Grigg GC, Seebacher F, Franklin CE), pp. 135–143, Surrey Beatty and Sons: Chipping Norton.

Demes B (2007) *In vivo* bone strain and bone functional adaptation. *Am J Phys Anthropol* **133**, 717–722.

Demes B, Qin YX, Stern JT, et al. (2001) Patterns of strain in the macaque tibia during functional activity. *Am J Phys Anthropol* **116**, 257–265.

Erickson GM, Lappin AK, Vliet KA (2003) The ontogeny of bite-force performance in American alligator (*Alligator mississippiensis*). *J Zool* **260**, 317–327.

Erickson GM, Gignac PM, Steppan SJ, et al. (2012) Insights into the ecology and evolutionary success of crocodilians revealed through bite-force and tooth-pressure experimentation. *PLoS ONE* **7**, e31781.

Grosse IR, Dumont ER, Coletta C, et al. (2007) Techniques for modeling muscle-induced forces in finite element models of skeletal structures. *Anat Rec (Hoboken)* **290**, 1069–1088.

Herring SW, Scapino R (1973) Physiology of feeding in miniature pigs. *J Morphol* **141**, 427–460.

Herring SW, Rafferty KL, Liu ZJ, et al. (2001) Jaw muscles and the skull in mammals: the biomechanics of mastication. *Comp Biochem Physiol Part A* **131**, 207–219.

Hibbeler RC (2000) *Mechanics of Materials*. Upper Saddle River, NJ: Prentice Hall.

Holliday CM, Witmer LM (2007) Archosaur adductor chamber evolution: integration of musculoskeletal and topological criteria in jaw muscle homology. *J Morphol* **268**, 457–484.

Hylander WL (1977) *In vivo* bone strain in the mandible of *Galago crassicaudatus*. *Am J Phys Anthropol* **160**, 223–240.

Hylander WL (1979a) The functional significance of primate mandibular form. *J Morphol* **160**, 223–240.

Hylander WL (1979b) Mandibular function in *Galago crassicaudatus* and *Macaca fascicularis*: an *in vivo* approach to stress analysis of the mandible. *J Morphol* **159**, 253–296.

Hylander WL (1981) Patterns of stress and strain in the macaque mandible. In: *Craniofacial Biology*. Monograph No. 10, Craniofacial Growth Series. (ed. Carlson DS), pp. 1–35, Ann Arbor, MI: Center for Human Growth and Development.

Hylander WL (1984) Stress and strain in the mandibular symphysis of primates: a test of competing hypotheses. *Am J Phys Anthropol* **64**, 1–46.

Hylander WL, Crompton AW (1986) Jaw movements and patterns of mandibular bone strain during mastication in the monkey *Macaca fasicularis*. *Arch Oral Biol* **31**, 841–848.

Hylander WL, Johnson KR, Crompton AW (1987) Loading patterns and jaw movements during mastication in *Macaca fascicularis*: a bone-strain, electromyographic, and cineradiographic analysis. *Am J Phys Anthropol* **72**, 287–314.

Hylander WL, Ravosa MR, Ross CF, et al. (1998) Mandibular corpus strain in primates: further evidence for a functional link between symphyseal fusion and jaw-adductor muscle force. *Am J Phys Anthropol* **107**, 257–271.

Kupczik K, Dobson CA, Fagan MJ, et al. (2007) Assessing mechanical function of the zygomatic region in macaques: validation and sensitivity testing of finite element models. *J Anat* **210**, 41–53.

Kupczik K, Dobson CA, Crompton RH, et al. (2009) Masticatory loading and bone adaptation in the supraorbital torus of developing macaques. *Am J Phys Anthropol* **139**, 193–203.

Lieberman DE, Krovitz GE, Yates FW, et al. (2004) Effects of food processing on masticatory strain and craniofacial growth in a retrognathic face. *J Hum Evol* **46**, 655–677.

Liu ZJ, Herring SW (2000) Bone surface strains and internal bony pressures at the jaw joint of the miniature pig during masticatory muscle contraction. *Arch Oral Biol* **45**, 95–112.

Marinescu R, Daegling DJ, Rapoff AJ (2005) Finite-element modeling of the anthropoid mandible: the effects of altered boundary conditions. *Anat Rec A* **283**, 3000–3309.

Mazzetta GV, Cisilino AP, Blanco RE (2004) Distribución de ensiones durante la mordida en la mandíbula de *Carnotaurus sastrei* Bonaparte, 1985 (Theropoda: Abelisauridae). *Ameghiniana* **41**, 605–617.

Mazzetta GV, Cisilino AP, Blanco RE, et al. (2009) Cranial mechanics and functional interpretation of the horned carnivorous dinosaur *Carnotaurus sastrei*. *J Vertebr Paleontol* **29**, 822–830.

McHenry C, Clausen P, Daniel WJT, et al. (2006) Biomechanics of the rostrum in crocodilians: a comparative analysis using finite-element modeling. *Anat Rec A* **288**, 827–849.

Metzger KA, Daniel WJT, Ross CF (2005) Comparison of beam theory and finite-element analysis with *in vivo* bone strain data from the *Alligator* cranium. *Anat Rec A* **283**, 331–348.

Moazen M, Curtis N, O'Higgins P, et al. (2009) Biomechanical assessment of evolutionary changes in the lepidosaurian skull. *Proc Natl Acad Sci U S A* **20**, 8273–8277.

Molnar RE (1998) Mechanical factors in the design of the skull of *Tyrannosaurus rex* (Osborn, 1905). *Gaia* **15**, 198–218.

Moreno K, Wroe S, Clausen P, et al. (2008) Cranial performance in the Komodo dragon (Varanus komodoensis) as revealed by high-resolution 3-D finite element analysis. *J Anat* **212**, 736–746.

Panagiotopoulou O, Curtis N, O'Higgins P, et al. (2010) Modelling subcortical bone in finite element analyses: a validation and sensitivity study in the macaque mandible. *J Biomech* **43**, 1603–1611.

Panagiotopoulou O, Kupczik K, Cobb SN (2011) The mechanical function of the periodontal ligament in the macaque mandible: a validation and sensitivity study using finite element analysis. *J Anat* **218**, 75–86.

Pierce SE, Angielczyk KD, Rayfield EJ (2008) Patterns of morphospace occupation and mechanical performance in exant crocodilian skulls: a combined geometric morphometric and finite element modeling approach. *J Morphol* **269**, 840–864.

Plotnick RE, Baumiller TZ (2000) Invention by evolution: functional analysis in paleobiology. In: *Deep Time: Paleobiology's Perspective.* (eds Erwin DH, Wing SL), pp. 305–323, Lawrence: The Paleontological Society.

Porro LB, Holliday CM, Anapol F, et al. (2011) Free body analysis, beam mechanics, and finite element modeling of the mandible of *Alligator mississippiensis*. *J Morphol* **272**, 910–937.

Rafferty KL, Herring SW, Marshall CD (2003) Biomechanics of the rostrum and the role of facial sutures. *J Morphol* **257**, 33–44.

Rayfield EJ (2011) Strain in the ostrich mandible during simulated pecking and validation of specimen-specific finite element models. *J Anat* **218**, 47–58.

Rayfield EJ, Milner AC (2008) Establishing a framework for archosaur cranial mechanics. *Paleobiology* **34**, 494–515.

Rayfield EJ, Norman DB, Horner CC, et al. (2001) Cranial design and function in a large theropod dinosaur. *Nature* **409**, 1033–1037.

Rayfield EJ, Milner AC, Xuan VB, et al. (2007) Functional morphology of spinosaur 'crocodile-mimic' dinosaurs. *J Vertebr Paleontol* **27**, 892–901.

Reed DA, Porro LB, Iriarte-Diaz J, et al. (2011) The impact of bone and suture material properties on mandibular function in *Alligator mississippiensis*: testing theoretical phenotypes with finite element analysis. *J Anat* **218**, 59–74.

Ross CF (2001) *In vivo* function of the craniofacial haft: the interorbital 'pillar'. *Am J Phys Anthropol* **116**, 108–139.

Ross CF, Dechow PC, Iriarte-Diaz J, et al. (2011) *In vivo* bone strain and finite-element modeling of the craniofacial haft in catarrhine primates. *J Anat* **218**, 112–141.

Ross CF, Metzger KA (2004) Bone strain gradients and optimization in vertebrate skulls. *Ann Anat* **186**, 387–396.

Ross CF, Patel BA, Slice DE, et al. (2005) Modeling masticatory muscle force in finite element analysis: sensitivity analysis using principal coordinate analysis. *Anat Rec A* **283**, 288–299.

Ross CF, Berthaume MA, Dechow PC, et al. (2011) *In vivo* bone strain and finite-element modeling of the craniofacial haft in catarrhine primates. *J Anat* **218**, 112–141.

Rybicki EF, Mills EJ, Turner AS, et al. (1977) *In vivo* and analytical studies of forces and moments in equine long bones. *J Biomech* **10**, 701–705.

Schwenk K (2000) Tetrapod feeding in the context of vertebrate morphology. In: *Feeding: Form, Function, and Evolution in Terrestrial Vertebrates.* (ed. Schwenk K), pp. 3–20, San Diego: Academic Press.

Sinclair AG, Alexander RM (1987) Estimates of forces exerted by the jaw muscles of some reptiles. *J Zool London* **213**, 107–115.

Soons J, Herrel A, Genbrugge A, et al. (2010) Mechanical stress, fracture risk and beak evolution in Darwin's ground finches (Geospiza). *Philos Trans R Soc Lond B Biol Sci* **365**, 1093–1098.

Strait DS, Wang Q, Dechow PC, et al. (2005) Modeling elastic properties in finite-element analysis: how much precision is needed to produce an accurate model? *Anat Rec A* **283**, 275–287.

Strait DS, Richmond BG, Spencer MA, et al. (2007) Masticatory biomechanics and its relevance to early hominid phylogeny: an examination of palatal thickness using finite-element analysis. *J Hum Evol* **52**, 585–599.

Taylor MA (1992) Functional anatomy of the head of the large aquatic predator *Rhomaleosaurus zetlandicus* (Plesiosauria, Reptilia) from the Toarcian (Lower Jurassic) of Yorkshire, England. *Philos Trans R Soc Lond B Biol Sci* **335**, 247–280.

Therrien F, Henderson DM, Ruff CB (2005) Bite me: biomechanical models of theropod mandibles and implications for feeding behaviour. In: *The Carnivorous Dinosaurs.* (ed. Carpenter K), pp. 179–237, Bloomington: Indiana University Press.

Van Drongelen W, Dullemeijer P (1982) The feeding apparatus of *Caiman crocodilus*; a functional-morphological study. *Anat Anz* **151**, 337–366.

Verrue VL, Dermaut L, Verhegghe B (2001) Three-dimensional finite element modeling of a dog skull for the simulation of initial orthopaedic displacements. *Eur J Orthod* **232**, 517–527.

Walmsley CW, Smits PD, Quayle MR, et al. (2013) Why the long face? The mechanics of mandibular symphysis proportions in crocodiles. *PLoS ONE* **8**, e53878.

Weijs WA, De Jongh HJ (1977) Strain in mandibular alveolar bone during mastication in the rabbit. *Arch Oral Biol* **22**, 667–675.

Weishampel DB (1995) Fossils, function and phylogeny. In: *Functional Morphology in Vertebrate Paleontology.* (ed. Thomason JJ), pp. 34–54, Cambridge: Cambridge University Press.

Williams SH, Wall CE, Vinyard CJ, et al. (2008) Symphyseal fusion in selenodont artiodactyls: new insights from *in vivo* and comparative data. In: *Primate Craniofacial Function and Biology.* (eds Vinyard CJ, Ravosa MR, Wall CE), pp. 39–61, New York: Springer.

Williams SH, Vinyard CJ, Wall CE, et al. (2009) Mandibular corpus bone strain in goats and alpacas: implications for understanding the biomechanics of mandibular form in selenodont artiodactyls. *J Anat* **214**, 65–78.

Zapata U, Metzger K, Wang Q, et al. (2010) Material properties of mandibular cortical bone in the American alligator, *Alligator mississippiensis*. *Bone* **46**, 860–867.

Zar JH (1999) *Biostatistical Analysis.* Upper Saddle River, NJ: Prentice Hall.

Supporting Information

Additional Supporting Information may be found in the online version of this article:

Video S1. Anterior view of deformation of the FEM amplified 10 × during anterior biting.

Video S2. Anterior view of deformation of the FEM amplified 10× during posterior biting.